Applied Thermal Engineering 204 (2022) 117927

Contents lists available at ScienceDirect

Applied Thermal Engineering

journal homepage: www.elsevier.com/locate/apthermeng

Review: Surface orientation effects on Pool-boiling with plain and enhanced surfaces

Munonyedi Egbo, Mohammad Borumand, Yahya Nasersharifi, Gisuk Hwang *

Department of Mechanical Engineering, Wichita State University, Wichita, KS 67260, United States

ARTICLE INFO

Keywords:
Critical heat flux
Heat transfer coefficient
Surface structures
Two-phase heat transfer
Surface orientation

ABSTRACT

A Pool Boiling (PB) is crucial to safe and efficient operations in various applications such as thermoelectric power conversion, refrigeration, electronics, transportation, microfluidics, biomedical engineering, metallurgical industry, and space exploration. However, the poor counter-current flows near the heated surface limit the maximum PB cooling efficiency via a premature surface dryout, i.e., poor Critical Heat Flux (CHF) and Heat Transfer Coefficient (HTC). The two-phase flow substantially changes as the surface orientation deviates from the upward facing, leading to the CHF and HTC changes. This paper reviews the effects of surface orientation on the two-phase flows and their PB performance using various coolants for plain and engineered surfaces. This review includes both the experimental and theoretical approaches to understand HTC and CHF, including tailored two-phase flow for enhanced HTC and CHF. This review also discusses future research directions for engineered surface under different surface orientation.

1. Introduction

Pool Boiling (PB) heat transfer, also known as natural convective heat transfer with liquid–vapor phase change, has been under extensive investigation for several decades, and the continued research interests stem from its potential benefits in high heat flux passive thermal management applications such as modern electronics, heat exchangers, energy conversion, metallurgical industry, and space exploration systems. One advantage of nucleate PB heat transfer over the conventional single-phase cooling systems is the ability to dissipate high heat fluxes at a low temperature gradient by employing the latent heat of vaporization of the working fluid [1-10]. This leads to the outstanding operational reliability due to the simplicity of its design with little or no moving mechanical parts.

Early studies on PB heat transfer focused on the phenomenological understandings on the plain horizontal upward-facing surfaces [3,5,11-27]. One of the key technical challenges lie in the first upper limit of nucleate PB, also known as Critical Heat Flux (CHF), which is related to a premature surface dryout. This leads to a poor Heat Transfer Coefficient (HTC), causing a catastrophic system burnout. The CHF is mainly caused by the limited coolant supply to the heated surface due to the critical two-phase flow instability [28] and/or poor wetting [29]. To delay such a surface dryout, various engineered surfaces have been explored [30] including microporous coating/structures [20,24,31-33], hybrid nano-/micro-structures [16,34], rough surfaces [13,17,26,5,35], nano-coatings [27,36,37], and micro-channels/grooves [3,38-40] by primarily tailoring the two-phase flow and/or wetting. Note that the surface wettability tailors the various key PB fundamentals including the nucleate site density, vapor departure diameter/frequency, vapor morphology, vapor growth/merge, thin film evaporation near the vicinity of the vapor root, and etc, thereby influencing the HTC and CHF. The detailed discussions are found in the literature [15,41-45]. In addition, the two-phase flow is substantially changed by the surface orientation relative to the direction of the gravitational acceleration, which strongly influence both the CHF and HTC. The fundamental understandings of the tailored two-phase flow on the different surface orientations rather than the upward facing surface is crucial to robust system design and flexible operations for high-heat-flux thermal management systems [5].

In this paper, we comprehensively review the major findings on the effects of the boiling surface orientation on PB performance in the literature. This paper aims to provide not only the recent research progress, but also insights into innovative surface structures/design on PB enhancements for future research.

The remainder of this paper is organized as follows. Section 1.1 describes a typical PB experiment, including various regimes within the

* Corresponding author.
E-mail address: Gisuk.Hwang@wichita.edu (G. Hwang).

https://doi.org/10.1016/j.applthermaleng.2021.117927
Received 7 August 2021; Received in revised form 22 October 2021; Accepted 7 December 2021
Available online 17 December 2021

nucleate PB process. Section 1.2 includes backgrounds including basic terminologies on the surface orientation. The surface orientation effects on the PB for different working fluids using plain surfaces is presented in section 2, with water and other coolants such as FC-72, Helium, Isopropyl alcohol, Hydrofluoroether (HFE-7100), and Ethanol, presented in sections 2.1 and 2.2, respectively. Existing developed correlations of surface orientation effects on PB heat transfer are summarized in section 3. Surface orientation effects on PB for different engineered or enhanced surfaces are presented in section 4, with surface roughness modification and microporous coated surfaces, presented in sections 4.1 and 4.2, respectively. Other surface enhancements are presented in section 4.3. Finally, concluding remarks and future research directions are provided in sections 5 and 6, respectively.

1.1. Pool-boiling regime and experiment

The Pool Boiling (PB) involves the heat transfer from a heated surface (heat source) to a liquid pool (heat sink) via the process of liquid natural convection and liquid–vapor phase change [46,47]. At given pressure of the PB chamber, PB occurs when the heated surface temperature T_s is above the corresponding saturation temperature of the liquid coolant T_{lg}, and the difference between these two temperatures is known as the superheat or excess temperature, $T_s - T_{lg}$ [46,48-50]. The measure of PB is generally presented in the heat flux across the boiling surface q at given superheat T_s - T_{lg} as shown in Fig. 1. The bubble morphology and behavior change as the heat flux transferred through the boiling surface increases. During the early boiling stages (usually at 5 °C superheat for water), small, isolated bubbles are nucleated at preferred locations on the heated surface such as cavity and/or defects. These bubbles grow in size as the heat flux, q, increases and they detach from the heated surface by buoyancy force at a desired bubble size, i.e., isolated bubble regime [51]. As the heat flux increases, the bubble nucleation rate substantially increases for continued bubble detachment, forming bubble jets, i.e., bubble jet regime. A continued increase in the heat flux results in a transition to the coalesced bubble regime, as the isolated bubbles and jets begin to merge and form a wavy vapor layer between the heated surface and liquid pool, and PB occurs primarily through the wetting fronts of the liquid waves at the liquid-surface interface. Due to the limited liquid supply to the heated surface, the HTC decreases. As the heat flux increases, the spotty dry patches form on the heated surface, which in turn results in the HTC reduction by the poor liquid supply to the heated surface. This is also known as a partial surface dryout. A further increase in the heat flux causes the heated surface to be covered by an excessive vapor, so called vapor blanket, which leads to a dramatic increase in the superheat at given heat flux, i.e., Critical Heat Flux (CHF).

A typical PB experimental setup is shown in Fig. 2(a). The heated surface is in contact with the liquid pool and the excessive heat is cooled by condenser to return the coolant to the liquid pool. An auxiliary temperature controller is used to control the liquid pool temperature. Typically, data acquisition units and a digital display screen are used to measure the temperatures of the heated surface, liquid pool, and heater. Note that the heat flux can be measured by the temperature gradient. However, in case that it is challenging to measure the reliable temperature gradient, direct heat flux senor can be used, especially in the cases that the integrity of the heater insulation is poor or that it is difficult to precisely determine small temperature differences [11,53-56].

To characterize PB heat transfer, the steady-state heat flux and the surface superheat are measured up to CHF where a sudden surface temperature rise occurs. Note that the steady-state heat flux is typically measured when the heated surface temperature and heat flux variations are small, i.e., < 5%, during 5–10 min. The HTC is calculated as the ratio of the steady-state heat flux to the superheat as given in Eq.(2). Note that some studies choose to measure the heat transfer effectiveness using the overall thermal resistance which is given as the reciprocal of HTC.

$$\Delta T = T_s - T_{lg} \tag{1}$$

$$\mathrm{HTC} = \frac{q}{\Delta T} \tag{2}$$

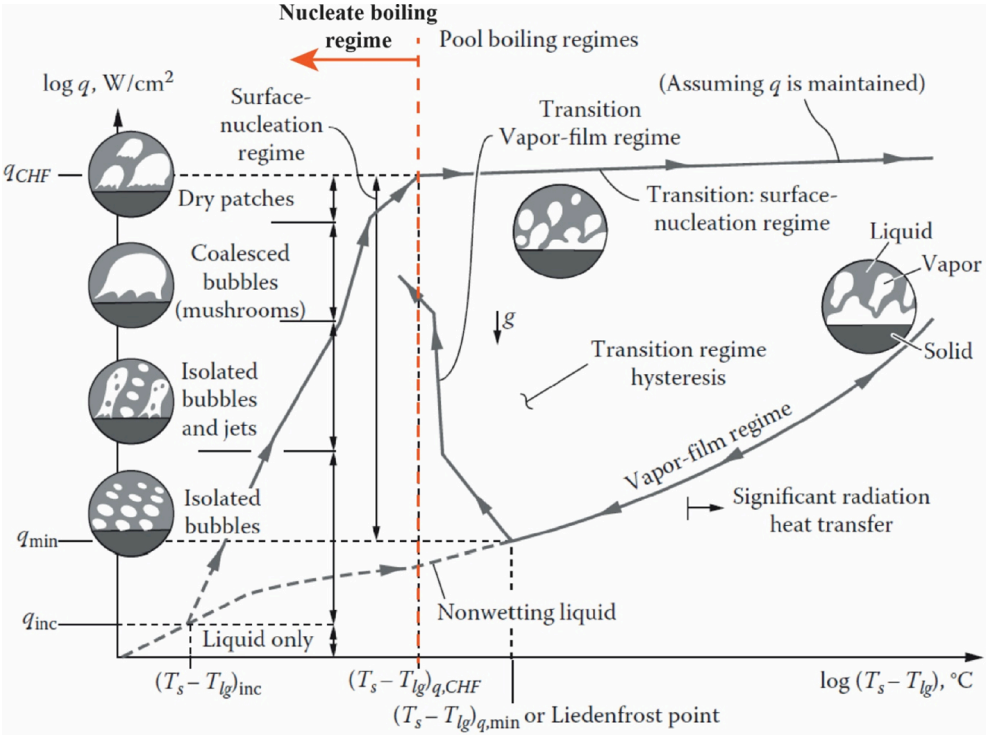

Fig. 1. Bubble morphology and regimes in pool boiling presented as variations of heat flux with respect to the superheat [51,52].

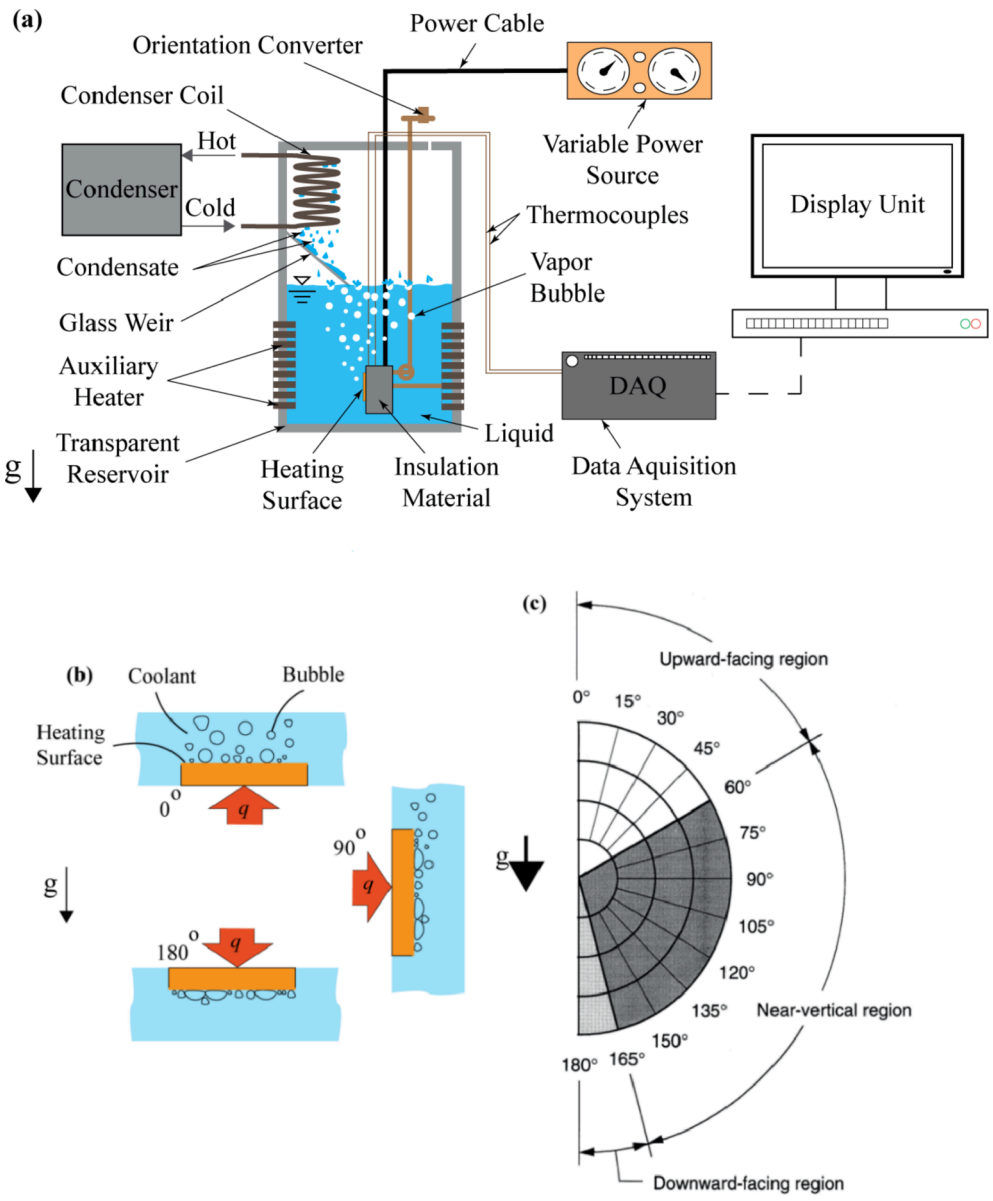

Fig. 2. (a) Schematic diagram of a typical pool-boiling experimental setup. The thermocouples are used to measure the heat flux and heated surface temperature. The data acquisition system, display unit, variable power source, auxiliary heater, and the condenser are also shown. (b) Horizontal upward-facing, 0°, vertical, 90°, and horizontal downward-facing, 180° surface orientations. The bubble dynamics are different at different orientations due to the influence of gravitational force. (c) Nucleate pool-boiling regions based on experimental observation of vapor dynamics at near-CHF heat fluxes [57].

1.2. Surface orientation

The heated surface orientation is usually specified as an angle from the gravitational acceleration direction, i.e., 0° for the upward-facing, 90° for the vertical, and 180° for the downward-facing surfaces [Fig. 2 (b)]. However, Howard and Mudawar [57] also categorized the surface orientations based on two-phase flow mechanisms at near CHF rather than physical surface orientation, such as (1) upward-facing region, (b) near-vertical region, and (c) downward-facing region [Fig. 2(c)].

1.3. Working fluid

The selection of the working fluid is critical to the desired operating temperature range, the chemical compatibility with the pool-boiling chamber, thermal/chemical stabilities, safety such as flammability and toxicity, and environmental impact. The key thermophysical properties

Table 1
Summary of the thermophysical properties of typical working fluids at ambient pressure [58,59].

Coolant	Saturation temperature, T_{lg} (°C)	Heat of evaporation, h_{lg} (kJ/kg)	Liquid density, ρ_l (kg/m^3)	Vapor density, ρ_g (kg/m^3)	Liquid viscosity, μ_l (10^{-6}N-s/m^2)	Liquid thermal conductivity, k_l (W/m-K)	Liquid surface tension, σ (10^{-3}N/m)
Water	100	2251.2	958.8	0.5974	279	0.680	58.91
Helium	−269	20.90	128.0	10.000	29	0.0277	0.09
FC-72	56	95.02	1594.0	13.130	436	0.057	84.10
Acetone	56.25	517.0	744.0	2.370	226	0.168	18.6
Ammonia	–33.3	1369.0	681.4	0.8972	273	0.615	33.9
Ethanol	78.3	960.0	759.0	1.430	432	0.169	17.3
Methanol	64.7	1130.4	755.5	0.1006	347	0.202	19.3

of the working fluids include the heat of evaporation, liquid and vapor densities, thermal conductivity, and surface tension, which are given in Table 1. Water is a preferred coolant in pool boiling heat transfer for several reasons. First, it has a relatively large latent heat of vaporization compared to most of the other cooling fluids (see Table 1), and therefore can be used in high-heat-flux applications. Secondly, the toxicity is very low, and its abundance leads to being readily available and affordable. Thirdly, water is thermally and chemically stable, and is very compatible with copper which is common PB surface. However, in applications operating at low-heat-flux, low operation temperature, and light weight, e.g., aerospace, other coolants such as liquid helium and FC-72 with low saturation temperature and density are alternatives to water.

2. Plain surface with different surface orientations

This section reviews the PB heat transfer on the plain surface with different surface orientations using various coolants such as water and other fluids, e.g., FC-72, Helium, Isopropyl alcohol, Hydrofluoroether (HFE-7100), and Ethanol as found below. The following two subsections (water and other fluids) are organized based on the working fluid types in literature, rather than the different PB physics from the different fluid types.

2.1. Water

Ishigai et al. [60] and Katto et al. [61] first studied the effects of surface orientation using saturated water on plain surfaces. Ishigai et al. [60] measured the upper limit of nucleate PB heat flux and the minimum film boiling heat flux in downward-facing copper surface with diameters of 25 and 50 mm, to compare with the upward-facing PB results. They reported that the CHF on the downward-facing surface is significantly lower than that of upward-facing surface, since the accumulated vapor bubble layer prevents the liquid access to the heated surface. Note that they did not explicitly state the percentage of this difference in CHF for the two surface orientations. Katto et al. [61], on the other hand, studied PB on vertically-oriented 10-mm-diameter copper surfaces using saturated water, and they showed the reduced CHF and HTC compared to the upward-facing surface due to the increased residence time of the generated bubbles on the boiling surface.

Marcus and Dropkin [62] studied PB with the 0 to 90° surface orientations at 22.5° intervals using a copper block with a surface area of 50.8×50.8 mm^2 and saturated distilled water. The experimental setup consisted of two nested glass containers, 2 and 12 Gal, respectively, an immersion heater for auxiliary heating, thermocouples, and a boiling surface mounted on a rotatable pin, and the schematic of their arrangements were as shown in Fig. 3.

They reported that the variation of the surface orientation from 0 to 90° increased the HTC by>20% as shown in Fig. 4. At an incipient boiling condition, $q = 0.0962$ W/cm^2, the highest HTC was observed at the horizontal upward-facing orientation. However, at higher heat fluxes, $1.67 \leq q \leq 11.2$ W/cm^2, the HTC increased with the increased surface orientation angle. This was attributed to the increased path length of the departing bubbles and a consequent enhancement in the bubble agitation per unit bubble, despite the decreased nucleation site density with increased surface orientation. For the normalized HTC by the HTC at 0° surface orientation at given heat flux i.e., h_θ/h_0, they reported that the normalized HTC does not change significantly with heat flux for boiling, whereas it changes significantly with heat flux at single-phase natural convection at lower heat fluxes. They observed a transition point, i.e., a point where h_θ/h_0 changes from decreasing to increasing. They concluded that there needs a transition heat flux above which the ratio h_θ/h_0 becomes insensitive to the heat flux.

Nishikawa et al. [63] also carried out an experimental study on the nucleate PB using water at ambient pressure to investigate the effects of the surface orientation on CHF and HTC. The heating surface was a 175 $\times$ 42 mm^2 copper plate. Two guide plates were installed on the longitudinal edges of the heating surface to ensure a one-dimensional bubble flow, i.e., minimum edge effects. PB experiment was carried out in both increasing and decreasing heat flux conditions, and no significant differences were observed, i.e., no hysteresis.

It was observed that at low heat fluxes, the heat flux curve shifts upwards as the surface orientation changes from 0° to 175°, indicating that the HTC increases with the surface orientation as shown in Fig. 5(a). However, they showed the similar boiling curves at high heat fluxes, claiming that the changes in the characteristics of the bubble behavior and the heat transfer mechanism are responsible for these observations in the nucleate boiling heat transfer performance with surface orientation.

Using the bubble characteristics, i.e., the nucleation site density and average diameter, they explained that at low heat fluxes, the nucleation site density decreases, and the bubble diameter increases as the surface orientation increases, while at high heat fluxes, the bubble generation is extremely vigorous that the coalesced bubbles cover the entire heating surface for any surface orientation. Nishikawa et al. [63] further identified two heat transfer mechanisms. One is the sensible heat transfer, responsible for the removal of the thermal layer adjacent to the heating surface by the elongated bubble rising, and the other is the latent heat transfer due to the evaporation of thin film beneath the elongated bubbles. They stated that while the stirring action of isolated bubbles controls the HTC in the low heat flux region at surface orientation below

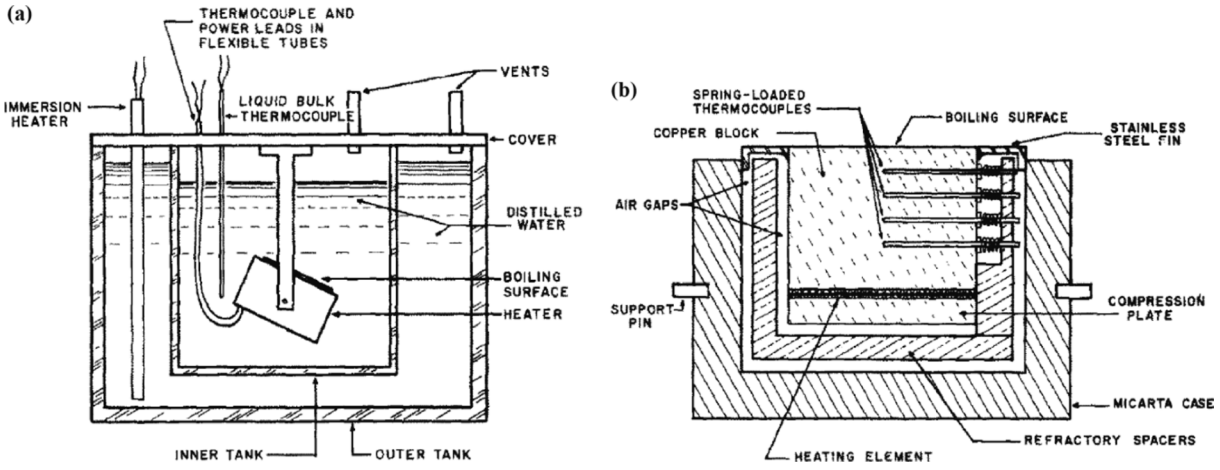

Fig. 3. (a) Schematic of the test cell showing the position of the boiling surface in relation to the test vessel. (b) Schematic detail of the heater and boiling surface showing the spring-loaded thermocouple installation and the heating arrangement [62].

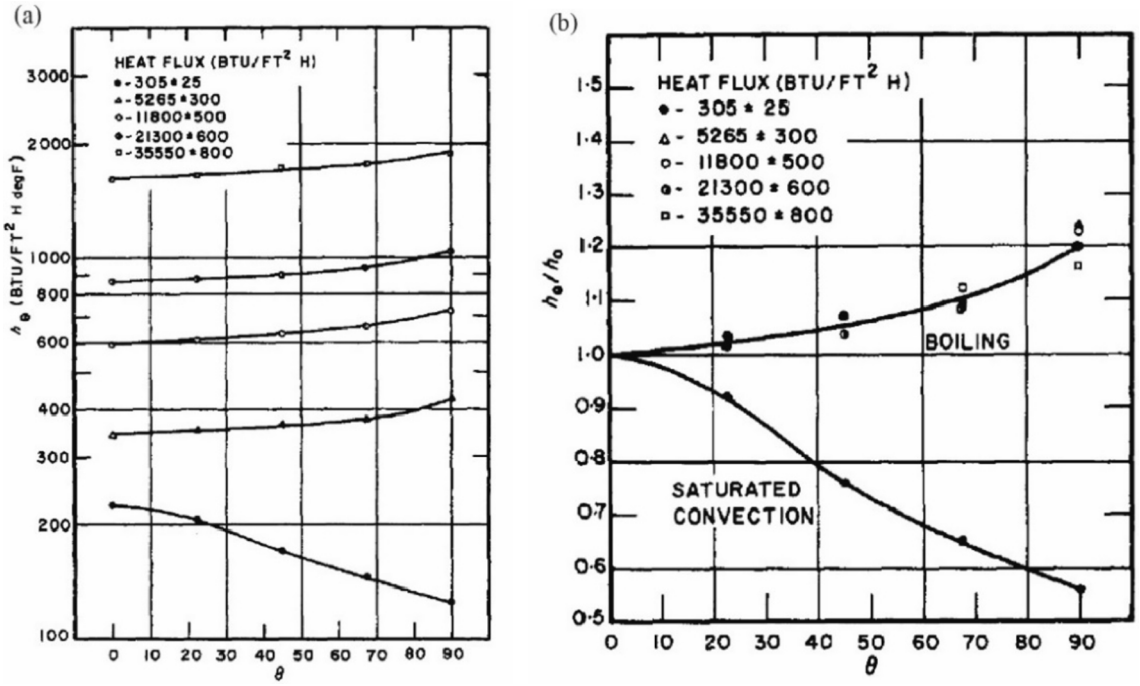

Fig. 4. (a) Heat transfer coefficient against the surface orientation for saturated convection and at different heat fluxes. (b) Ratio of h_θ/h_o against θ for saturated convection and at different heat fluxes. $\theta = 0$ represents the horizontal surface [62].

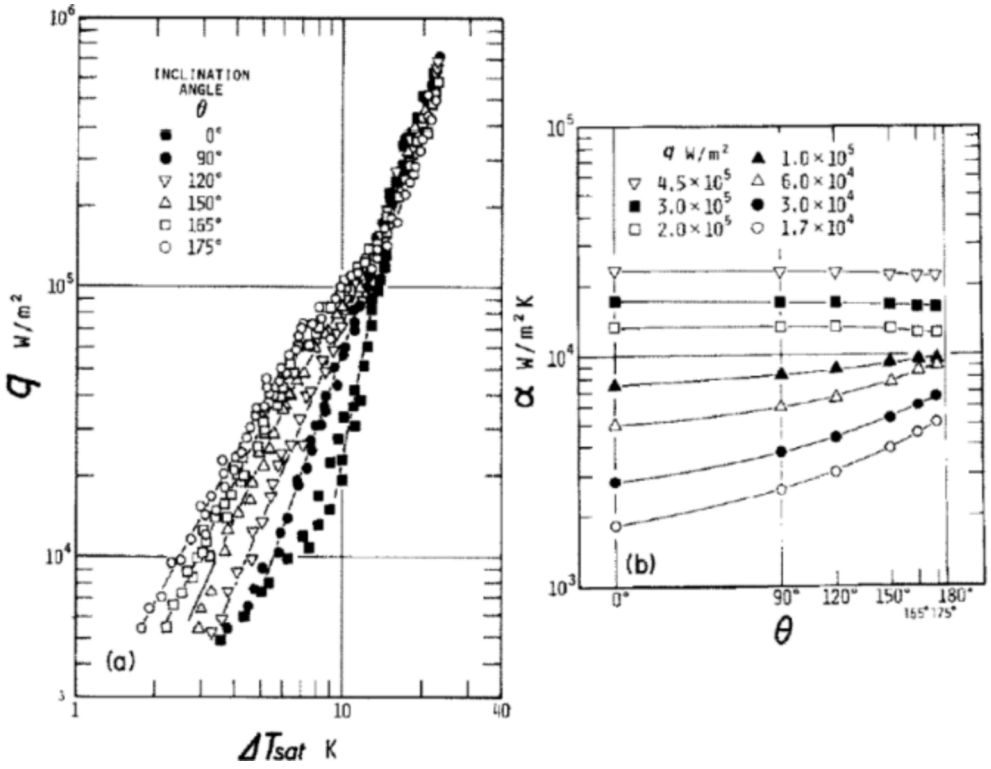

Fig. 5. (a) Heat flux as a function superheat for different surface orientations, and (b) heat transfer coefficient as a function surface orientations at given heat fluxes [63].

120°, the two aforementioned heat transfer mechanisms dominate at surface orientation above 150°. Also, they classified the nucleate boiling region into three: (a) the low heat flux region where the effect of changing the surface orientation is significant, (b) the high heat flux region where changing the surface orientation disappears, and (c) the middle heat flux region where the effect of surface orientation disappears asymptotically. They concluded that the heat transfer at an inclined downward-facing surface, i.e., >90° is controlled mainly by the latent heat transfer, using the developed analytical model.

Recently, Guo and El-Genk [64] studied PB on surface orientations

above 90° by quenching 50.8 mm diameter copper disk in saturated water at near-ambient pressure. Their study was motivated by (1) the need for the chemical industry to properly handle hazardous and highly flammable fluids such as propane, ethylene, and ammonia, in the case of railroad and storage tank fire outbreaks, and (2) the possible use of water as a coolant in the reactor cavity of Pressurized Water Reactors (PWRs). It was reported that the nucleate boiling always started at the lowermost position of the inclined surface before propagating upwards and that the quenching time for the downward-facing surface was 6 and 23 times that of the surface inclined at 175 and 90°, respectively. The variations of the quenching time with the exposed surface orientation of the copper disk further proved the dependence of surface orientation on pool-boiling heat transfer.

Gribov et al. [65] studied the heat transfer and upper limit of heat flux in the nucleate PB of water at saturated condition, at 135, 150, 165, and 175° orientations using a 10 × 110 mm^2 stainless steel plate. They reported that each surface orientation produced different boiling curves and CHF, observing that the CHF decreased as the surface orientation increased from 135 to 175°. Granovskii et al. [66] also carried out a similar study for the downward-facing orientation only, i.e., 180° using 200 × 100 mm^2 12Kh18N10T stainless steel surface with distilled water. The generated vapor was removed horizontally along the longer side of the heating surface. They reported that both the heat transfer effectiveness and the CHF were lower than conventional horizontal upward-facing heating surfaces of similar surface dimensions. Based on their visual observations and theoretical derivations, they concluded that the CHF occurs when the liquid supply rate is smaller than the vapor production rate.

Chu et al. [67] examined the boiling curve of relatively large downward-facing surfaces using a quenching test for two cylindrical samples with a diameter of 61 cm. One had a flat surface, while the other had a curved surface with a curvature radius of 335 cm. They reported that the boiling curves and the CHF were very similar, but the measured CHF, 50 W/cm^2, was smaller than the generally accepted CHF values for upward-facing surfaces, 100 – 130 W/cm^2, and larger than those obtained from correlations derived from smaller scale experiments.

Yang et al. [68] have studied the effects of heating surface size and orientation on the nucleate PB CHF. Four flat surface sizes, 20 × 200, 25 × 200, 30 × 150, and 40 × 150 mm^2 were tested at the surface orientations of 0, 30, 90, 120, 130, 150, 174, 176, 178, and 180° using saturated and slightly subcooled water at near-ambient pressure. In the near-saturated pool condition, two distinct regions were identified based on the CHF behavior; (a) the gradual change region where the CHF changed moderately with surface orientation, and (b) the steep change region where the CHF changed drastically with the surface angle. A transition point, which is the surface orientation between the gradual and steep change regions, was reported as 170°. In the slightly subcooled water, on the other hand, it was reported that the CHF increased as the surface orientation decreased from 180° to 0°. Yang et al. [68] also reported that a transition angle exist between 150° and 180°, and that the CHF decreased marginally and dramatically with the surface orientation below and above the transition angle.

Kang [69] demonstrated the effects of tube surface orientation on nucleate PB heat transfer of saturated water at near-ambient pressure. The experiments were performed for 0, 15, 30, 45, 60, 75, and 90°, using two stainless steel tube diameters of $D = 12.7$, and 19.1 mm and a fixed length of $L = 540$ mm. Their experimental results showed that the minimum and maximum HTCs were achieved when the tubes were in vertical and near-horizontal positions, and they found out that the decrease in the bubble slug formation on the tube surface and the easy liquid access to the surface could be the primary reasons for the enhancement, as similarly observed in the previous work [70].

More recently, Jung and Kim [71] have studied the effects of surface orientation on heat flux, HTC, nucleation site density, and bubble departure diameter to provide insights into the physical mechanism of nucleate PB heat transfer. They employed an optical visualization setup, and they integrated shadowgraph, total reflection, and infrared thermometry technique, as shown in Fig. 6, incorporating their results into the wall boiling model. Photographs of the PB and liquid-bubble phase distribution at constant wall superheat of 7.5 °C for various surface orientations are shown in Fig. 7.

They reported that the HTC increases as the surface orientation increases from 0 to 90° as shown in Fig. 8, concluding that the sliding effect of the bubbles along the inclined heating surface promotes larger active nucleation site density leading to more bubble generation and coalescence which results in larger HTC.

Jung and Kim [71] observed an increase in nucleation site density as the surface orientation angle increases, which is consistent with a previous study [72]. By calculating the thermal boundary layer thickness they explained that the increased nucleation site density is related to the increased thermal boundary layer thickness, which is in turn a result of the larger transient conduction due to the longer bubble residence at larger surface orientations, i.e., larger shear stress. They found that the average thermal boundary layer thickness for the latter was greater than that of the former, and it increased with the surface orientation as shown in Fig. 9(a). It was concluded that the thermal boundary layer increases the nucleation site density, and as a result, the enhanced HTC on the inclined surfaces is attributed to the larger average thermal boundary layer thicknesses, as shown in Fig. 9(b). The numbers of departing isolated bubbles decrease as the surface orientation increases because the nucleated and growing bubbles slide along the heating surface at inclined surface instead of direct bubble escape by the buoyancy. The bubble coalescence results in the increased average departing bubble diameter as shown in Fig. 9(c).

2.2. Other fluids

2.2.1. Perfluorohexane (FC-72)

Perfluorohexane, popularly known as FC-72, is a chemical compound that contains carbon and fluorine, and the pure FC-72 or its mixture with another fluid is used as coolant for electronic cooling applications due to its low boiling point, i.e., 56 °C, and high-wetting characteristics. FC-72 is alsorelatively inexpensive and safe to both biological beings and the environment [32,73]. These favorable thermophysical properties and characteristics motivated extensive studies on two-phase cooling systems using FC-72 as working fluid including nucleate PB, heat pipes, vapor chambers (flat heat pipes), and thermosiphons [74-86].

You [87] has concluded that the variations of the boiling curves at different orientation angles are associated with the nature of the nucleation sites and the difference between the generated vapor bubbles and the bulk liquid coolant. In their experiment, the heating surface was a 5 mm square platinum block on a glass substrate with inclination angles of 0, 90, 150, 175, and 180°.

Howard and Mudawar [57] carried out an extensive study on the effects of surface orientation on nucleate PB CHF of near-saturated FC-72 and PF-5052 to develop a mechanistic CHF prediction model for near-vertical surfaces. The experimental study involved an extensive flow visualization of PB at various surface orientations to understand the CHF trigger mechanisms for different surface orientations. They identified the CHF trigger mechanism for different surface orientations, and by incorporation of classical two-dimensional interfacial instability theory, a separated flow model, an energy balance, and a lift-off criterion, they were able to develop a theoretical-based CHF model capable of predicting the surface orientation effects. Two heaters, a 12.7 × 12.7 mm^2 and a 3.2 × 35 mm^2, were used. The PB test chamber was fabricated from G-10 fiberglass plastic and fitted with two Lexan windows for visualizing two-phase flows. The videos and still photographs were employed in recording the boiling events at various heat fluxes in the nucleate boiling regime until reaching CHF. They claimed that both the square and thin surfaces exhibited same general vapor behavior prior to CHF for all surface orientation angles, and based on the vapor behavior

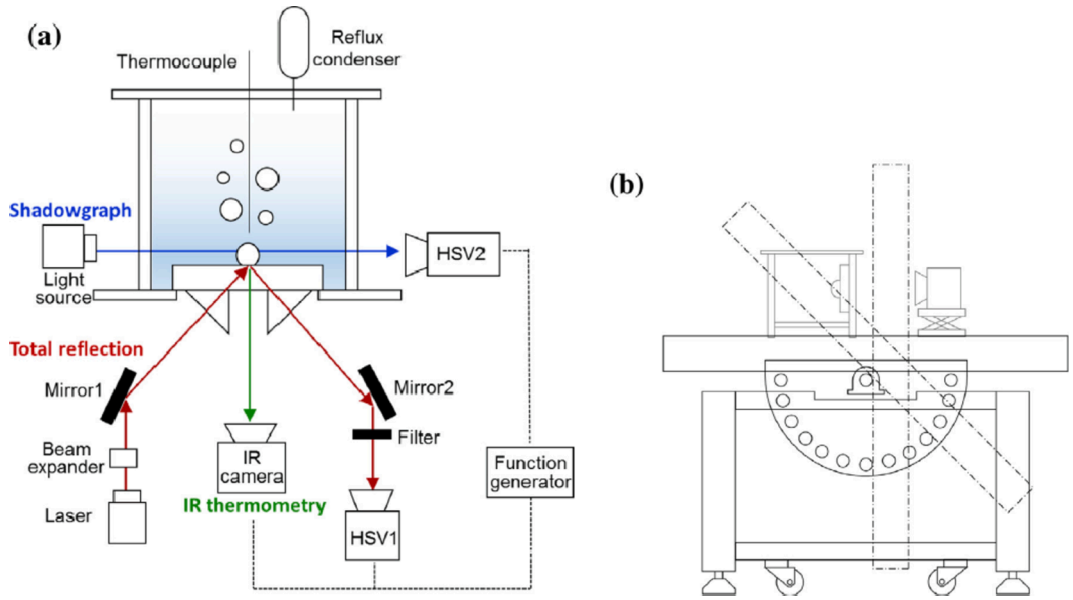

Fig. 6. Schematics of the (a) pool boiling experimental setup and (b) rotatable optical table to examine the effects of surface orientation [71].

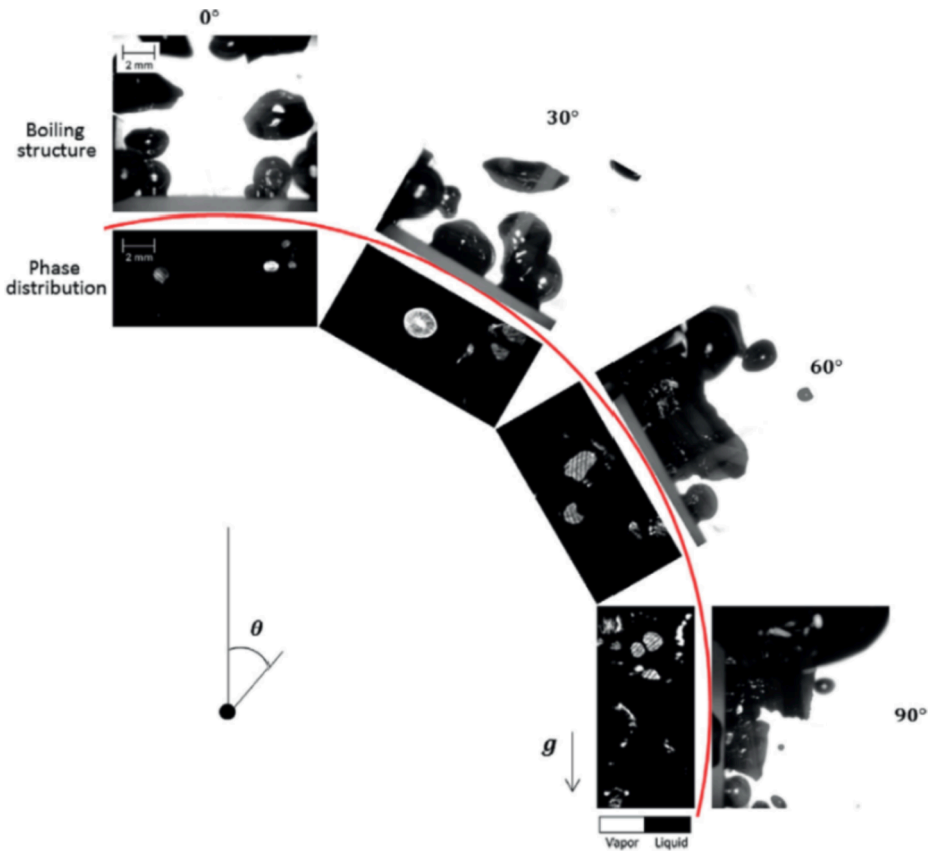

Fig. 7. Photographs of pool boiling and liquid–vapor phase distribution at the constant wall superheat of 7.5°C for various orientations [71].

at near-CHF heat fluxes, they divided the boiling process into three regions: (1) the upward-facing region, i.e., 0 to 60°, where the generated surface vapor departs vertically by buoyancy, (2) the near-vertical region, i.e., 60 to 165°, where the generated surface vapor slides along the hot surface and hydrodynamic instability causes the vapor–liquid interface to be wavy and eventually separate the wetting fronts from the hot surface, and (3) the downward-facing region, i.e., 165 to 180°, where the generated vapor is stratified along the heated surface, preventing liquid from reaching or rewetting the hot surface and eventually leading to complete surface dryout, as shown in Fig. 2(c).

They also provided a still photograph of the surface vapor prior to CHF in order to clearly substantiate their claim that vapor behavior at near-CHF was critical in providing more accurate CHF models that account for surface orientation, as shown in Fig. 10. The photographs showed clear distinction between the three boiling regions, with the upward-facing showing surface release of the generated vapor and the

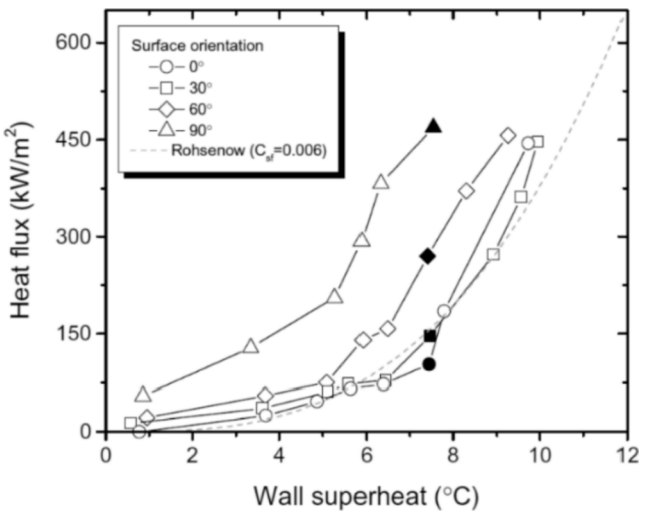

Fig. 8. Heat flux as a function of wall superheat for different surface orientations. Note that CHF was not achieved in each surface orientation as the study focused on HTC and bubble parameters [71].

downward-facing showing surface sliding movement. The sliding movement of the wavy vapor in the inclined upward-facing surfaces were occasionally disrupted by the vertical release of the vapor due to the combined effects of surface interaction and buoyancy. A transition angle between the near-vertical and the downward-facing regions was found to be around 165°, which is similar to a previous finding by Yang et al. [68] using saturated water. This shows that the transition angle between the near-vertical region, where wavy liquid–vapor interface exists, and downward-facing region, where vapor stratification is dominant, is independent of the type of fluid used in the nucleate PB process.

Based on the established vapor behaviors at various defined boiling regions, Howard and Mudawar [57] went further to develop a model capable of predicting nucleate PB CHF at different orientations, for near-vertical surfaces.

2.2.2. Helium

Helium is a low-boiling-temperature liquid, i.e., −269 °C at 1 atm, and is used not only in nucleate PB low-temperature heat transfer applications [88-92], but also in other delicate phase-change cooling systems, because of its low density and non-toxic nature.

Lyon [93] investigated the effects of orientation (0, 90 and 180°) on nucleate PB using helium. The experiment was carried out at different liquid temperatures from −271.39 to −268.02°C, and pressures from 6.0 to 288 kPa. They showed that at constant liquid temperature and pressure, the CHF decreases as the surface orientation increases from 0 to 180°. Bewilogua et al. [94] studied different liquids, including helium, over a wide range of pressures using a cryostat in a PB experiment. The effects of pressure on parameters such as bubble departure frequency and bubble departure diameter were examined using hydrogen and liquid nitrogen, while helium was used to investigate the dependency of the heat transfer on the surface orientation. The heater surface was a 2.5 cm diameter circular copper. They found that at given pressure ratio, p/p_c, the nucleate PB CHF decreases as the surface orientation increases from 0° to 165°, as shown in Fig. 11.

Bewilogua et al. [94] fitted the experimental data using Kutateladze's [95] correlation, i.e., Eq.(3) given as

$$q_m = Kh_{fg}\rho_v^{\frac{1}{2}}[\sigma g(\rho_l - \rho_v)]^{\frac{1}{4}} \tag{3}$$

where K is the fitting parameter, which is related to the surface

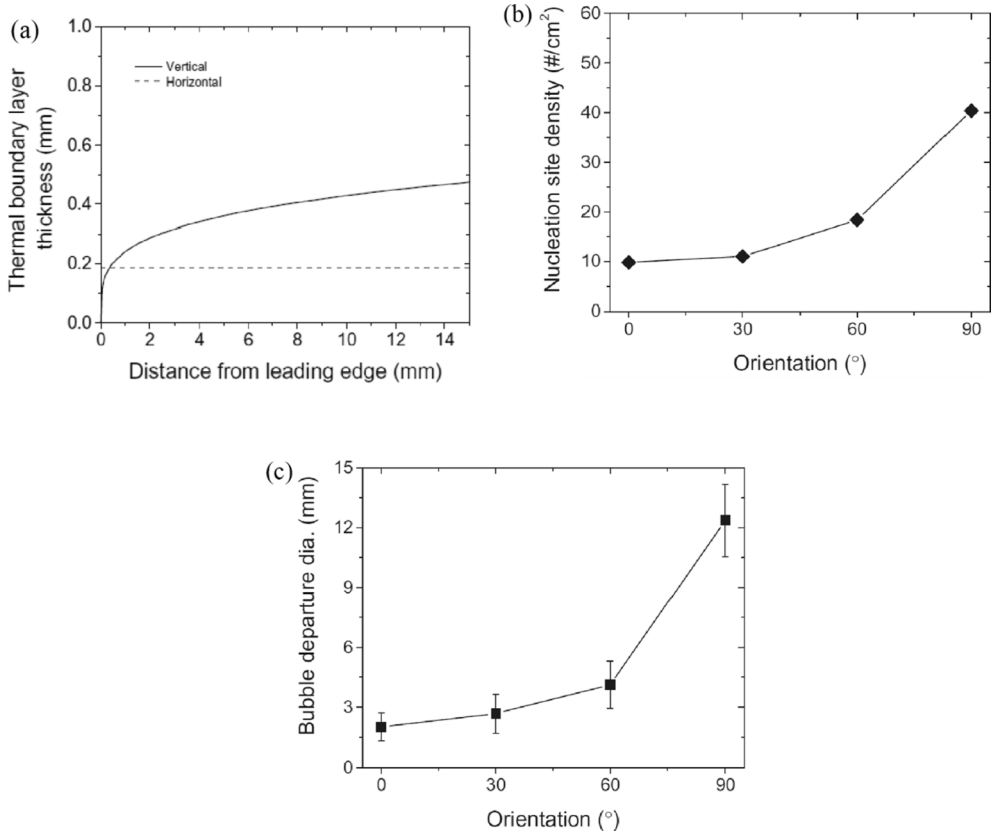

Fig. 9. (a) Predicted thermal boundary layer thickness on horizontal and vertical heater surfaces, (b) nucleation site density, and (c) bubble departure diameter as a function of surface orientation [71].

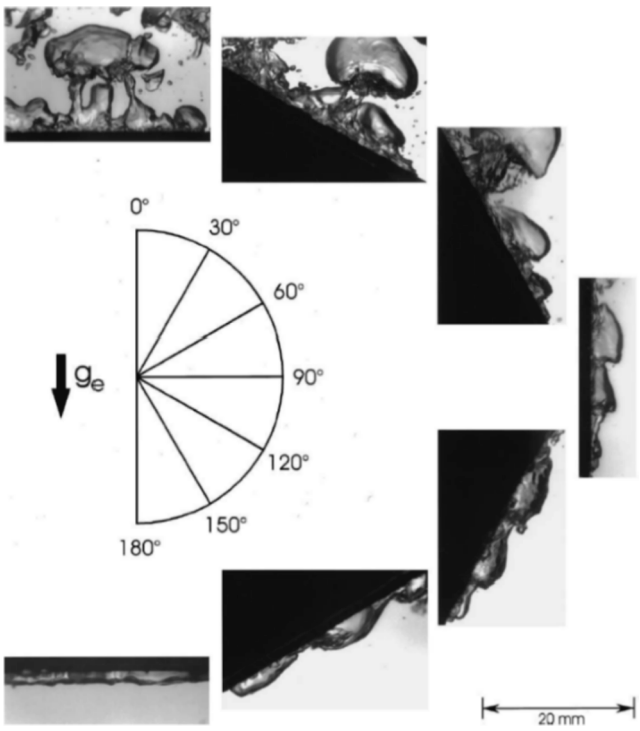

Fig. 10. Pool boiling photographs at different surface orientations for the thin heater [57].

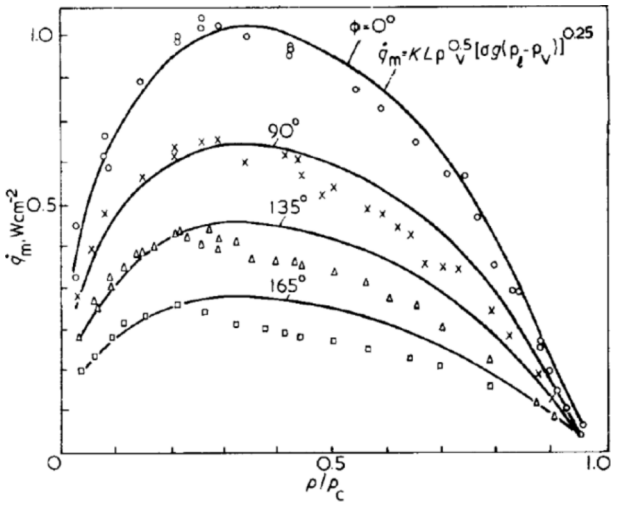

Fig. 11. Critical heat flux as a function of pressure ratio for different surface orientations using helium. Note that p and p_c are the total and critical pressure, respectively [94].

orientation ϕ, and it was derived from the previous work [96], given as

$$K = 0.016(190 - \phi)^{\frac{1}{2}} \tag{4}$$

Jergel and Stevenson [97] carried out a nucleate PB experiment on a 15 mm diameter aluminum surface, Al 59, at three different surface orientations, 0, 90, and 180° using saturated helium at ambient pressure. They recorded a CHF of 1.41, 0.92, and 0.2 W/cm^2 for the 0, 90, and 180° orientations, respectively, as shown in Fig. 12. They also compared the experimental results on Al 59 with their previous work using oxygen-free high thermal conductivity (OFHC) copper surface [98], showing a similar trend in CHF, albeit at the same surface orientation, the latter had higher HTC than the former, as shown in Fig. 12.

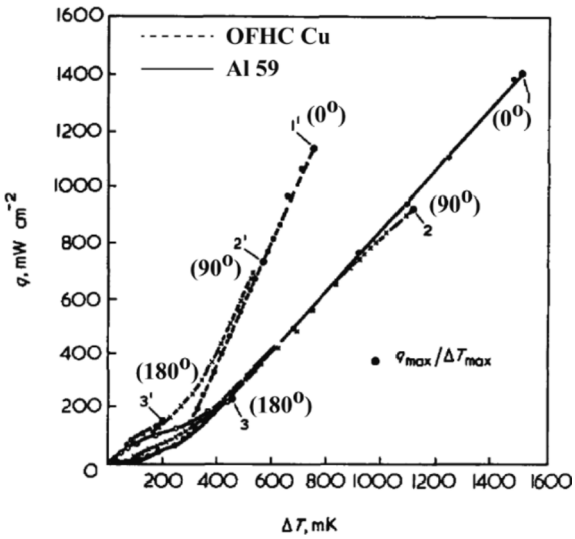

Fig. 12. Heat flux versus wall superheat for helium at different surface orientations [97].

2.2.3. Isopropyl alcohol, Hydrofluoroether (HFE-7100), and Ethanol

Other liquid coolants have been examined on the surface orientation dependent nucleate PB heat transfer including isopropyl alcohol, cyto-fluorometer, also known as HFE-7100, and ethanol for desired operation conditions and minimal environment impacts, i.e., global warming.

Githinji and Saberskey [99], as far back as 1963, investigated the surface-orientation dependent nucleate PB performance using subcooled isopropyl alcohol under ambient pressure. They used a 101.6 (length) × 3.175 (width) × 0.0254 (thickness) mm^3 chromax strip, with the 101.6 (length) × 3.175 (width) mm^2 plain area as a boiling surface. As shown in Fig. 13, their nucleate PB experiment shows that the HTC for the vertical surface was moderately larger than that of 0° surface orientation, but far larger than that of 180° surface orientation, which is similar to that of the single-phase natural convection in the downward-facing surface orientation. Their visual observations also revealed that the bubbles form a thermal blanket, i.e., covering the heating surface with vapor layer at 180° surface orientation, and that the bubble dynamic behaviors do not contribute to the convection heat transfer mechanism as they do for other surface orientations.

Misale et al. [100] selected narrow spaces to study the effects of surface inclination on nucleate PB heat transfer and CHF using a dielectric fluid hydrofluoroether (HFE-7100). The heating surface was a copper disk, approximately 3 cm in diameter, confined by a face-to-face parallel insulated (adiabatic) surface. The surface orientation varied from 0 to 135° with a 45° increment while confinement gaps (widths) were selected as 0.5, 1.0, 2.0, 3.5, 5.0, 10.0, and 20 mm. For channel widths larger than 3.5 mm, the CHF behavior was found to be similar to

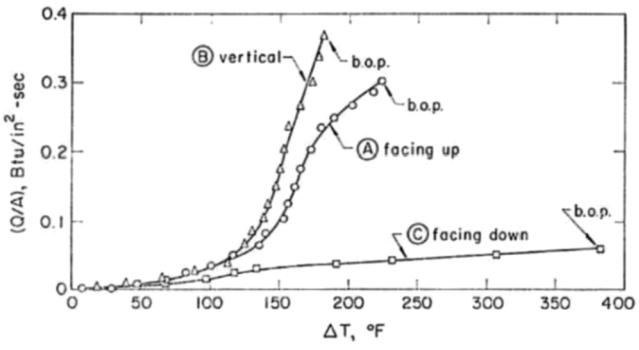

Fig. 13. Heat flux as a function of wall superheat. The end points of each of the boiling curves is known as "burn out point" (b.o.p) [99].

those exhibited by unconfined PB surfaces, with the maximum CHF at 0° and decreasing as the surface orientation increases from 0 to 135°, as shown in Fig. 14(a)–(c). Misale et al. [100] also found that for channel widths smaller than 3.5 mm, the CHF decreases as the channel width decreases, and that the magnitude of the reduction was dependent on the surface orientation. They reported that the 0° surface yielded the maximum reduction in CHF, and that the largest CHF gradually moved towards the 90° surface. For channel width of 3.5 mm, the maximum CHF occured at 45°. They also presented the normalized CHF data for the confined (0.5, 1.0, 2.0, and 3.5 mm) and unconfined surfaces at various surface orientations to clearly show the CHF enhancements at given surface orientations for different channel widths.

Gogonin and Kutateladze [101] have conducted an experimental study that investigated the boiling of ethanol using a flat stainless-steel surface at horizontal upward- and downward-facing surface orientations, i.e., 0° and 180°. The width of the rectangular heating surface (150 mm in length) was varied from 5 to 50 mm. Their results showed that the CHF for the 180° surface was far less than that of the 0° surface, for the same surface width and pressure, although they did not explicitly state the percentage of this difference. They also attributed the lower CHF of the latter to the difficulty of bubble escape from the heated surface, which in turn led to bubble coalescence and the premature formation of vapor blanket on the heated surface.

El-Genk and Bostanci [102] have employed a 10 mm × 10 mm copper surface to study the effects of surface inclination on nucleate PB using HFE-7100. It was reported that at low heat fluxes, the HTC increases as the surface orientations increases from 0 to 150° but decreases drastically as the surface orientation increases from 150 to 180°. However, the CHF decreases slightly between 0 and 90° and drastically between 90 and 180°. They also reported the CHF of 24.45 and 4.30 W/cm^2 for the 0 and 180° surface orientations, respectively, and also explained their results by comparing with similar observed bubble dynamics that was reported in previous works by Jun et al. [103] and Howard and Mudawar [57], as shown in Fig. 15.

A summary of the key observations on the effects of surface orientation on nucleate pool-boiling heat transfer for plain surface using different working fluids is presented in Table 2.

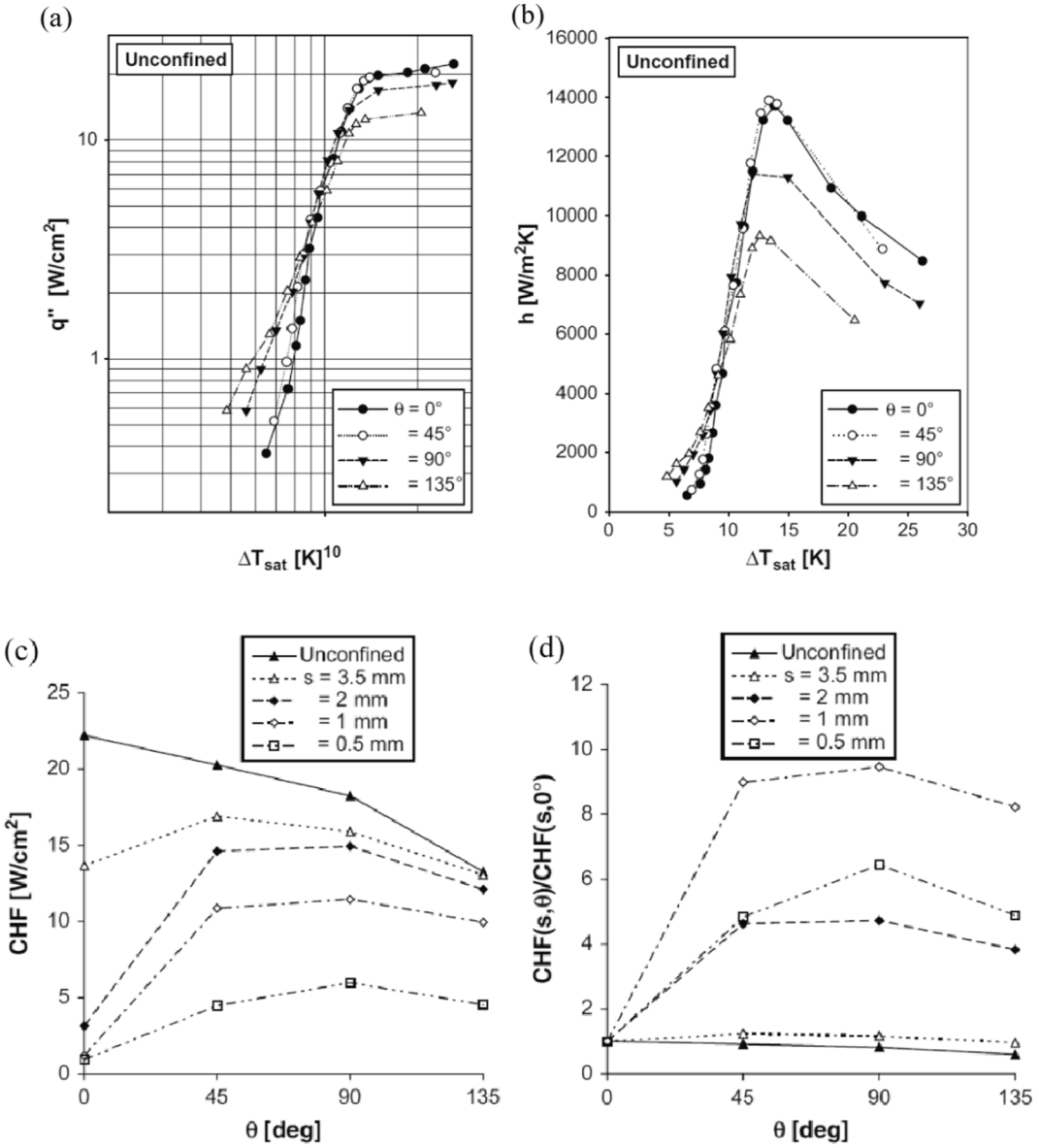

Fig. 14. (a) Heat flux as a function of wall superheat for unconfined surface, (b) heat transfer coefficient as a function of wall superheat for unconfined surface, (c) CHF versus surface orientation for both confined and unconfined surfaces, (d) CHF normalized with the CHF at 0° orientation angle at different surface orientations [100].

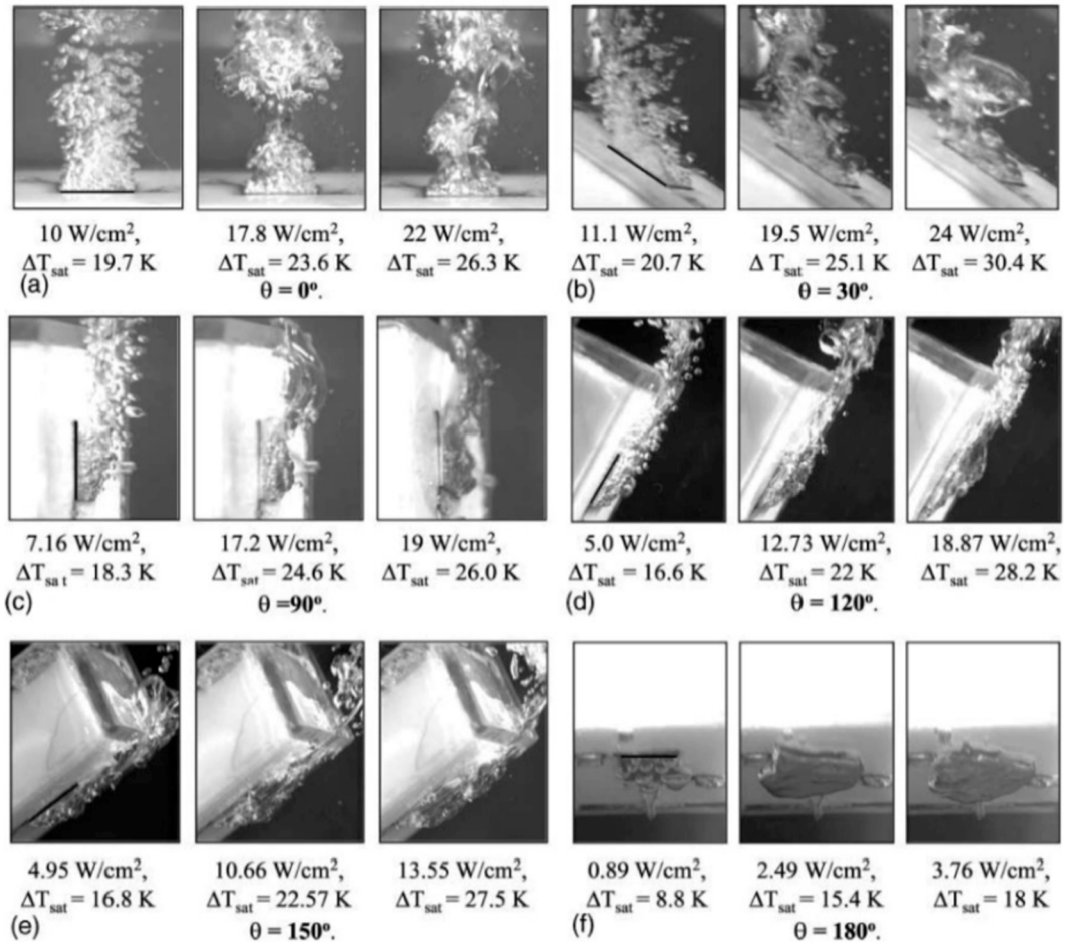

Fig. 15. Photographs of saturated nucleate pool boiling of HFE-7100 at different surface inclinations [102].

2.3. Summary

An interim summary on the PB surface orientation effects on plain surface is given as: (1) CHF decreases as the boiling surface orientation angle increases from horizontal upward facing (0°) to horizontal downward facing (180°). Between 0 and 90°, the decrease in CHF was less pronounced than the decrease in CHF between 90 and 180°. (2) HTC increases as the boiling surface orientation angle increases from horizontal upward facing (0°) to the vertical position (90°) but decreases above 90°. (3) The changes on the CHF and HTC with respect to the boiling surface orientation are related to the bubble dynamics.

3. Predictions

3.1. Heat transfer coefficient (HTC)

Rohsenow developed a HTC correlation on the plain, horizontal upward-facing surface, which is known as Rohsenow correlation, given as [104]

$$\frac{c_p(T_w - T_s)}{h_{fg}Pr^s} = C_{sf}\left[\frac{q}{\mu h_{fg}}\sqrt{\frac{\sigma}{g(\rho_f - \rho_v)}}\right]^{0.33} \tag{5}$$

where Pr is the Prandtl number, C_{sf} and s are constants determined by the heater surface condition and working fluid properties [104]. This is a widely used HTC correlation, but it predicts only on the horizontal surface. The HTC on the horizontal surface is further elaborated based on the phase-change phenomena near the boiling surface, so called basic wall boiling model, developed by Kurul and Podowski [105]. The total heat flux from the wall to the liquid is partitioned into three components, given as

$$q''_w = q''_e + q''_q + q''_c \tag{6}$$

where q_e is the evaporative heat flux related to the latent heat flux required to form the bubbles, q_q is the quenching heat flux which is a transient conduction heat flux required to reform the thermal boundary layer, and q_c is the convective heat flux which is transferred to the liquid phase outside the bubble influence area. The basic wall boiling model is formulated using the wall temperature and bubble parameters such as the nucleation site density and bubble departure diameter as crucial variables, however, the values of all of the bubble parameters are expressed as functions of only temperature [106-108] without considering the surface orientation. To reasonably predict the HTC on surfaces with orientation, Jung and Kim [71] incorporated the effects of merging of isolated bubbles due to buoyancy on the inclined surface by introducing a reduction factor, R, given in Eq.(7), on the basis of their experimental observations [71], and successfully predicted their experimental data on various orientation angles ($0° < \theta < 90°$).

$$R = \frac{1/N''}{0.25\pi D^2_{d,\,merge}} \tag{7}$$

where N" is the nucleation site density and $D_{d,merge}$ is the average diameter of the departing merged bubble. Therefore, for a tilted surface the evaporative heat flux in Eq.(6) can be found using Eq.(8)

$$q''_e = RN''f\left(\pi D^3_{d,\,merge}\right)\rho_g h_{fg} \tag{8}$$

Table 2
Summary of the key observations on the effect of surface orientation on nucleate pool-boiling heat transfer for plain surface using different working fluids.

Reference	Surface description/ Chamber pressure	Surface orientation (°)	Key observation(s)
Water (H_2O)			
Ishigai et al. [60]	25 and 50-mm-diameter copper surfaces/1 atm	180°	Both the HTC and CHF at 180° surface orientation are significantly lower than at 0°
Katto et al. [61]	10-mm-diamter copper surface/3.0–46.5 kPa	0 and 90°	The CHF and HTC at 90° are slightly less than that of a 0° oriented surface
Marcus and Dropkin [62]	50.8 × 50.8 mm^2/1 atm	0 − 90° at 22.5° intervals	At high heat fluxes, the HTC increases with the surface orientation due to the increase in the number of active nucleation sites
Nishikawa et al. [63]	175 × 42 mm^2 rectangular surface/1 atm	0, 90, 120, 150, 165, and 175°	At low heat fluxes, the HTC increases with the surface orientation, however, at high heat fluxes the HTC are similar at each surface orientation
Guo and El-Genk [64]	Copper, 50.8 and 12.8 mm in diameter and thickness, respectively/ 1 atm	90, 135, 150, 165, 170, 175, and 180°	The quenching time for the 180° surface is 6 and 23 times that of a surface oriented at 175 and 90°, respectively
Gribov et al. [65]	10 × 110 mm^2 stainless steel plate with a thickness of 0.1 mm/1 atm	135.150, 165, and 175°	Different surface orientations produce different boiling curves
Granovskii et al. [66]	200 × 100 mm^2 stainless steel surface with a thickness of 1 mm/1 atm	180°	Both the HTC and CHF are low compared those reported for horizontal upward-facing surfaces
Chu et al. [67]	Two solid cylindrical masses, each with a diameter and thickness of 61 cm and 10 cm, respectively/1 atm	180°	The observed CHF, 50 W/cm^2, is smaller than the generally accepted CHF values for upward-facing surfaces, 100 – 130 W/cm^2 but larger than those obtained from derived correlations from smaller scale experiments
Yang et al. [68]	Four flat surface sizes, 20 × 200 mm^2 and 25 × 200 mm^2, 30 × 150 mm^2 and 40 × 150 mm^2/1 atm	0, 30, 90, 120, 130, 150, 174, 176, 178, and 180°	CHF increases as the surface orientation decreases from 180 to 0°
Jung and Kim [71]	Not specified/1 atm	0, 30, 60, and 90°	HTC increases as the surface orientation increases from 0 to 90°, due to the increased nucleation site density
Other Fluids			
Perfluorohexane (FC-72)			
You [87]	5 mm × 5 mm/1 atm	0, 90, 150, 175, and 180°	The heat transfer performance is related to the bubble dynamic which is influenced by the surface orientation
Howard and Mudawar [57]	12.7 mm × 12.7 mm, 3.2 × 35 mm^2 (thin heater)/1 atm	0, 30, 60, 90, 120, 150, and 180°	CHF decreases as the surface orientation increases from 0 to 180°, while HTC increases between 0 and 90°, and then decreases between 90 and 180°
Liquid Helium (He)			
Lyon [93]	9.91-mm-diameter platinum surface/ 6.0–288 kPa	0, 90, and 180°	Maximum and minimum CHF is achieved at 0 and 180° surface orientations, respectively
Bewilogua et al. [94]	2.5 cm circular copper surface/1 atm	0, 90, 135, 165, and 180°	CHF decreases as the surface orientation increases from 0 to 180°
Jergel and Stevenson [97]	15 mm diameter Aluminuim disk/1 atm	0, 90, and 180°	CHF of 1.41, 0.92, and 0.2 W/cm^2 for the 0, 90, and 180° surface orientations, respectively
Isopropyl alcohol, Hydrofluoroether (HFE-7100), and Ethanol			
Reference	Surface description/ Chamber pressure/ Working fluid	Surface orientation (°)	Key observation(s)
Githinji and Saberskey [99]	101.6 mm × 3.175 mm /1 atm/Isopropyl alcohol	0, 90, and 180°	HTC is maximum and minimum at surface orientation of 90 and 180°, respectively
Misale et al. [100]	3 cm diameter/1 atm/ Hydrofluoroether (HFE-7100)	0, 45, 90, and 135°	CHF decreases as the surface orientation increases from 0 to 135°
Gogonin and Kutateladze [101]	Stainless-steel, Length – 150 mm, width (5–50 mm)/(10–520) μPa/ Ethanol	0 and 180°	CHF of the 180° oriented surface is far less than that of a 0° surface
El-Genk and Bostanci [102]	10 mm × 10 mm copper surface/1 atm/HFE-7100	0, 30, 60, 90, 120, 150, and 180°	CHF decreases as the surface orientation increases from 0 to 180°; almost linearly between 0 and 90°, and drastically between 90 and 180°

where f is the bubble departure frequency, ρ_g is the vapor density, and h_{fg} is the latent heat of evaporation. Note that the reduction factor, R, is always greater than unity and results in increased evaporative heat flux, q_e, as orientation angle increases from 0 to 90°.

Fig. 16 shows the predicted wall heat flux using the modified wall boiling model as a function of surface orientation indicating an RMS error of 44% compared to the experimental data [71]. Fig. 16 shows the contribution of the individual heat flux to the total heat flux, and the quenching heat flux is dominant in the upward-facing horizontal surface ($q_e/q_w \sim 80\%$), however, as the surface is inclined toward vertical, the contribution of the evaporative heat flux becomes increasingly dominant ($q_w/q_e \sim 80\%$ at $\theta = 90°$), which is in line with the experimental

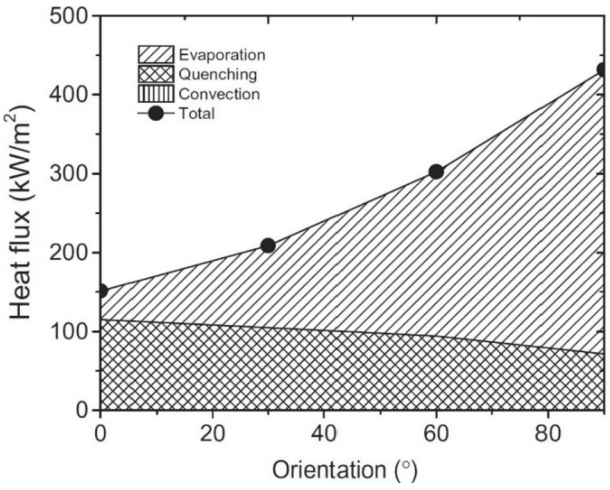

Fig. 16. Predicted individual heat fluxes, namely evaporation, quenching, convection, as a function of surface orientation using the modified wall boiling model [71].

observations [71]. Note that the contribution of the convective heat flux, q_c, is minimal compared to q_e and q_w.

3.2. Critical heat flux (CHF)

The CHF model has been originally developed for the horizontal surface orientation, 0°, and it has been modified for other surface orientations. Kutateladze [109] has developed a CHF correlation for the 0° surface using saturated liquid, given as

$$\frac{q_{\mathrm{CHF}}}{\rho h_{fg}\left[\frac{\sigma(\rho_f-\rho_g)g_e}{\rho_g^2}\right]^{\frac{1}{4}}}=K \tag{9}$$

where K is the dimensionless Critical Heat Flux (CHF), and 0.16 best fits into the experimental results. Zuber et al. [110] has combined principles of the Helmholtz and Taylor hydrodynamic instability to improve the Kutaleladze's correlation and reported $K = 0.131$ for an infinite horizontal surface. However, Eq.(9) does not predict the CHF for vertical surface orientation, i.e., 90° ($g = 0$). To predict the CHF for different surface orientations, i.e., $0° < \theta < 90°$, Mudawar et al. [111] performed photographic and video imaging studies for near-saturated PB with FC-72 and water, showing that the CHF on the vertical surface is only 13% smaller than that of the horizontal surface. They found out that the CHF triggering mechanisms on the vertical surface are similar to those of vapor production and flow patterns for flow boiling rather than the horizontal PB CHF. For vertical surfaces, the Kelvin-Helmholtz instability creates a wavy liquid–vapor layer with individual sweeping wave troughs, so called wetting fronts, and the curvature of the individual wetting fronts preserves the interfacial contact. They postulated that the CHF occurs when the lifting force by the vapor exceeds the pressure force from the interfacial contact, i.e., interfacial lift-off model. The interfacial lift-off model incorporates a separated flow model, an energy balance, classical two-dimensional interfacial instability theory, and a criterion for separation of the wavy vapor interface. A force balance at the most upstream wetting front yields

$$\rho_g\left[\frac{q_l}{\rho_g h_{fg}\left(1+c_{p,f}\Delta T_{sub}/h_{fg}\right)}\right]^2=\overline{p_f-p_g} \tag{10}$$

where q_l is the localized heat flux in the wetting front. The average pressure difference due to the interfacial curvature is given as

$$\overline{p_f-p_g}=2\sqrt{2}\pi\frac{\sigma\delta}{\lambda_{cr}^2} \tag{11}$$

where λ_{cr} is the critical wavelength corresponding to onset of Helmholtz instability and δ is the mean vapor layer thickness. For a vertical surface, analytical expressions for the mean vapor layer thickness δ and the critical wavelength λ_{cr} are obtained using the separated flow, which yields

$$\delta=\frac{q''_{\mathrm{CHF}}}{\rho_g h_{\mathrm{fg}}(1+c_{\mathrm{p,f}}\Delta T_{\mathrm{sub}}/h_{\mathrm{fg}})}\left\{g\left(\frac{\rho_{\mathrm{f}}-\rho_{\mathrm{g}}}{\rho_{\mathrm{g}}}\right)\frac{q''_{\mathrm{CHF}}}{0.5f_i\rho_g h_{\mathrm{fg}}(1+c_{\mathrm{p,f}}\Delta T_{\mathrm{sub}}/h_{\mathrm{fg}})}\right\}^{-1/3}\lambda_{\mathrm{cr}}^{2/3} \tag{12}$$

$$\lambda_{cr}=[2\pi\sigma(\frac{\rho_{\mathrm{f}}+\rho_{\mathrm{g}}}{\rho_{\mathrm{f}}\rho_{\mathrm{g}}})]^{3/5}\left\{g\left(\frac{\rho_{\mathrm{f}}-\rho_{\mathrm{g}}}{\rho_{\mathrm{g}}}\right)\frac{q''_{\mathrm{CHF}}}{0.5f_i\rho_g h_{\mathrm{fg}}(1+c_{\mathrm{p,f}}\Delta T_{\mathrm{sub}}/h_{\mathrm{fg}})}\right\}^{-2/5} \tag{13}$$

where $f_i = 0.5$ is the interfacial friction factor. Therefore, the critical heat flux is given as

$$q_{\mathrm{CHF}}=2^{-113/24}3^{5/6}\left(\frac{\pi}{f_i}\right)^{1/4}\left(\frac{\rho_f}{\rho_f+\rho_g}\right)\rho_g h_{fg}\left(1+\frac{c_{p,f}\Delta T_{sub}}{h_{fg}}\right)\left[\frac{\sigma(\rho_f-\rho_g)g}{\rho_g^2}\right]^{\frac{1}{4}} \tag{14}$$

Eq.(14) can be further simplified for the near-saturated conditions to yield the following analytical expression for CHF on vertical surfaces

$$q_{\mathrm{CHF}}=0.151\rho_g h_{fg}\left[\frac{\sigma(\rho_f-\rho_g)g}{\rho_g^2}\right]^{\frac{1}{4}} \tag{15}$$

which is identical in form, but not in mechanism, to traditional horizontal CHF models given in Eq.(9). Howard and Mudawar [57] extended their previous work [111] by performing experiments with different fluids such as liquid helium and covering a wider range of surface orientations. They showed that the interfacial lift-off trigger mechanism identified in [111] can also be applied for all near-vertical surface orientations, i.e., $60° < \theta < 165°$ with respect to the upward-facing surface. However, unlike the case for vertical surface, here an iterative numerical scheme should be employed to calculate CHF due to unavailability of an analytical expression for δ and λ_{cr}. Therefore, the following expression for CHF on near-vertical surfaces ($60° < \theta < 165°$) is formulated [57].

$$q_{\mathrm{CHF}}=0.25\rho_g\Delta h_{fg}\left(1+\frac{c_p\Delta T_{sub}}{\Delta h_{fg}}\right)\left[2\sqrt{2}\pi\frac{\sigma\delta}{\rho_g\lambda_{cr}^2}\right]^{1/2} \tag{16}$$

Fig. 17 compares the existing experimental CHF results for FC-72 with the predictions of Eq.(16). Eq.(16) reasonably predicts the decreasing CHF with increasing surface orientation at $60° < \theta < 130°$, however, it begins to deviate from the experimental data as the surface orientation approaches the downward facing regime, i.e., $\theta > 130°$

Kandlikar [29] has developed a theoretical model to describe the hydrodynamic behaviors of the vapor–liquid interface of a single bubble at the heated surface leading to the CHF for $0° < \theta < 90°$. He included the effects of surface-liquid interaction through the dynamic receding contact angle and tested the model for water, refrigerants, and cryogenic liquid. The CHF for near-saturated and subcooled conditions can is given in Eqs.(17) and (18), respectively

$$qsat_{\mathrm{CHF},}=\rho_g^{0.5}h_{fg}\left(\frac{1+cos\beta}{16}\right)\left[\frac{2\sigma}{D_b}(\rho_f-\rho_g)g_e\frac{D_b}{4}(1+cos\beta)cos\theta\right]^{\frac{1}{2}} \tag{17}$$

$$q_{CHF,sub}=q_{\mathrm{CHF},sub}\left(1+\frac{\Delta T_{sub}}{\Delta T_{sat}}\right) \tag{18}$$

where β and D_b are the contact angle and the bubble diameter. Kandlikar [29] showed that CHF initiates once the force parallel to the heater

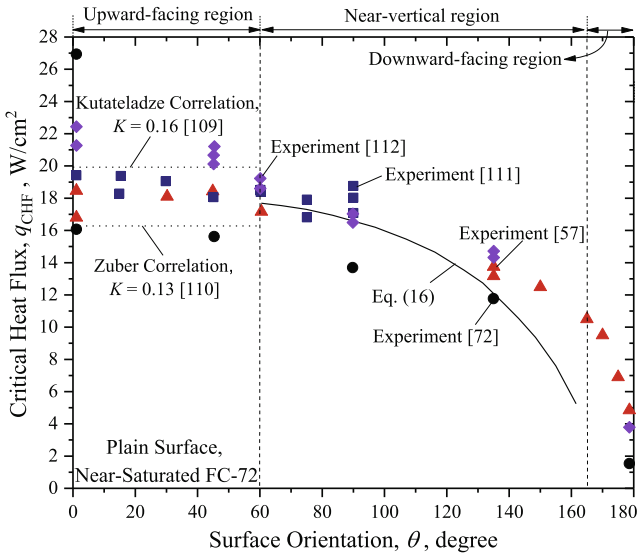

Fig. 17. Comparison of CHF model predictions in the near vertical region, i.e., Eq.(16) [57], with experimental data for FC-72 [57,72,109-112].

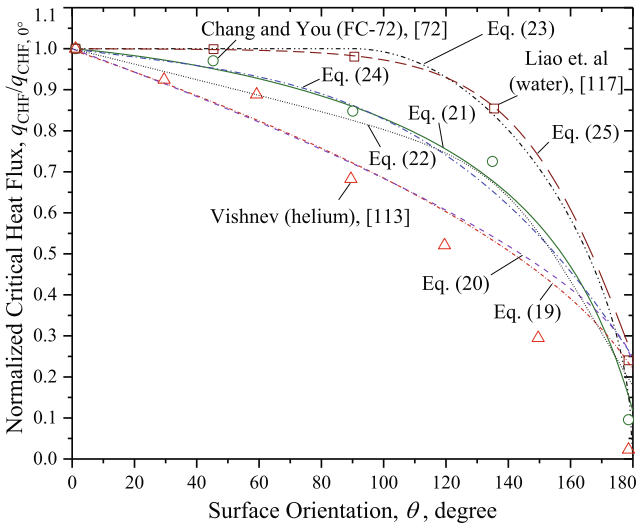

Fig. 18. Predicted, normalized CHF, $q_{CHF}/q_{CHF,0°}$ as a function of surface orientation using Eqs.(19)-(25), see Table 3. Experimental results are also shown [72,113,117].

surface resulting from the evaporation at the liquid–vapor interface of a bubble near the heater surface exceeds the retaining forces due to gravity and surface tension, which is highly influenced by the receding contact angle.

Various CHF empirical correlations for different working fluids and heating surfaces (area, structure, geometry, etc.) at different surface orientations are given in Table 3. It is obvious that none of these empirical models can be used to accurately predict PB CHF for different working fluid, surface characteristics, and PB working conditions (e.g., chamber pressure and pool temperature). An analytical or semi-analytical model could be potentially used, however, the knowledge gaps in the present understanding of liquid–vapor behavior of PB as well as the random behavior in the bubble–liquid–vapor interactions have presently hindered any significant progress in developing an analytical or semi-analytical CHF model.

Fig. 18 shows the normalized CHF as a function of surface orientation for the correlations, Eqs.(19)–(25) found in Table 3, and three sets of experimental results using FC-72 [72], Helium [113], and water [117]. The normalized CHF non-linearly decreases with increasing surface orientation, and the correlations predict the rate of decreasing CHF differently. Eqs.(23) and (25) predict minimal decrease in CHF as the surface orientation θ increases from 0° to 90° followed by a sharp CHF decrease for $\theta > 90°$, which reasonably agree with the experimental results using water [117]. On the other hand, Eqs.(21), (22), and (24) predict the moderate CHF reduction between 0° to 90°, and the rate of CHF decrease becomes significant as the surface orientation θ increases above 90°, which agree with the experimental results using FC-72 [72]. Eqs.(19) and (20) predict near-linear CHF reduction, especially for $0° < \theta < 130°$, which are in line with the experimental results using helium [113]. In short, the different rate of the CHF decrease is related to the different working fluids due to the different thermophysical properties, and no universal relation exists to predict surface orientation dependant CHF reduction. Table 4 summarizes the key observations of the effects of surface orientation on nucleate pool-boiling heat transfer for enhanced surface using different working fluids.

3.3. Summary

An interim summary on the predictive model on CHF and HTC for the PB surface orientation effects is given as: (1) For the model for HTC, only one study using the modified wall model predicts the available experimental data as a function of surface orientation within an RMS error of 44% [71]. However, this model compares with only one study case, and further studies are needed to improve the model accuracy by including different surface condition and thermophysical property effects, etc. (2) Several surface-orientation dependent models based on the experimental results using helium, water, and dielectric fluids predict the CHF reduction as the surface orientation increases from horizontal upward

Table 3
Generated correlations that describe the effects of heating surface orientation on nucleate PB CHF.

Reference/Surface type	Fluid	Correlation	
Vishnev [113]/Plain	Helium	$q_{CHF} = q_{CHF,0°}\left[\frac{190-\theta}{190}\right]\frac{1}{2}$	(19)
El-Genk and Guo [114]/Plain	Water	$q_{CHF} = \left[0.034 + 0.0037(180-\theta)^{0.656}\right] h_{fg}\left[\rho_g^2 g\sigma(\rho_l-\rho_g)\right]^{\frac{1}{4}}$	(20)
Chang and You [72]/2D enhanced	FC-72	$q_{CHF} = q_{CHF,0°}[1.0 - 0.0012\theta tan(0.414\theta) - 0.122sin(0.318\theta)]$	(21)
El-Genk and Bostanci [102]/Plain	HFE-7100	$q_{CHF} = \left[(0.229-4.27\times10^{-4}\theta)^{-6} + (0.577-2.98\times10^{-3}\theta)^{-6}\right]^{-\frac{1}{6}} \times \rho_g h_{fg}\left[\sigma g\frac{(\rho_f-\rho_g)}{\rho_g^2}\right]^{\frac{1}{4}}$	(22)
Brusttar and Merte [115]/Plain	R-113	$q_{CHF} = \begin{Bmatrix} q_{CHF,0°}, & 0°\leqslant\theta\leqslant90° \\ q_{CHF,0°}(sin\theta)^{0.5}, & 90°\leqslant\theta\leqslant165° \end{Bmatrix}$	(23)
Arik and Bar-Chohen/ [116]/Plain	HFE-7100 and FC-72	$q_{CHF} = q_{CHF,0°}\left[1 - 0.001117\theta + 7.79401\times10^{-6}\theta^2 - 1.37678\times10^{-7}\theta^3\right]$	(24)
Liao et al. [117]/2D enhanced	Water	$q_{CHF} = q_{CHF,0°}\left[-0.73 + \frac{1.73}{1+10^{-3.8934+0.021\theta}}\right] \times \left[1 + \frac{55-\beta}{100}(0.56-0.0013\theta)\right]$	(25)

Table 4
Summary of the key observations of the effects of surface orientation on nucleate pool-boiling heat transfer for enhanced surface using different working fluids.

Reference	Surface description/Chamber pressure/Working fluid	Surface orientation (°)	Key observation(s)
Surface roughness/Microcavities			
Deev et al. [132]	square copper heater, 30 mm × 30 mm/1 atm/Helium	0 and 90°	HTC does not vary with the surface orientation
Nishio and Chandratilleke [133]	Copper surface, 20 mm in diameter/1 atm/Helium	0, 45, 90, 135, 157, 175, and 179°	At low heat flux, the HTC increases as the surface orientation increases from 0 to 175°. CHF decreased as the surface orientation increases
Microporous Coatings			
Chang and You [72]	10 mm × 10 mm/1 atm/Water	0, 45, 90, 135, and 180°	CHF decreases as the surface orientation increases
Rainey and you [31]	1 cm^2, 4 cm^2, and 25 cm^2 square heaters/1 atm/FC-72	0, 45, 90, 135, 160, and 180°	CHF decreases as the surface orientation increases
Jun et al. [103]	Two enhanced copper surfaces, each 1 × 1 cm^2/ 1 atm/Water	0, 45, 90, 135, and 180°	CHF increases slightly as the surface orientation increases from 0 to 90°, but it decreases above 90°
Other surface enhancements			
Jung et al. [136]	Plain circular disk, 78 mm in diameter/2 bar/R-11	0, 45, 90, 135, 150, 165, 170, and 180°	Within the nucleate boiling regime, the wall superheat decreases by 15–25% as the surface orientation changes from 0 to 165°
Reed and Mudawar [112]	12.7 mm square heater/1 atm/FC-72 and FC-87	0, 45, 90, 135, and 180°	CHF decreases as the surface orientation increases
Kim and Suh [137]	15 mm × 15 mm rectangular copper surface, coated with thin film of nickel to prevent oxidation/1 atm/Water	90−180°, with about 10° pace	CHF decreases with the surface orientation. The transition angle is dependent on the confinement/gap size
Liao et al. [117]	Three 20-mm-diameter copper surfaces with different wettability/1 atm/Water	0, 45, 90, 135, and 180°	CHF decreases with the surface orientation for each of the surfaces, slightly between 0 and 90° and dramatically above 90°
Narayan et al. [139]	Tubular heating surface, 33 mm and 170 mm in diameter and length, respectively/1 atm/Water-alumina nanofluid	0, 45, and 90°	The 0 and 45° surface orientation achieved the maximum and minimum HTC, respectively
Kwark et al. [134]	100 mm^2 surface coated with 139 nm particle/1 atm/Water	0, 45, 90, 135, and 180°	At low heat fluxes, the HTC increases with the surface orientation. However, at high heat fluxes, the boiling is similar. The CHF decreases as the surface orientation increases

facing (0°) to downward facing surfaces (180°). However, the model predictions significantly deviate from the experimental results $60° < \theta < 160°$, while they reasonably agree to the experimental results near the horizontal upward facing (0°) and downward facing surfaces (180°). Further studies are need to improve the accuracy of the surface orientation dependent CHF for different types of working fluids.

4. Enhanced boiling on engineered oriented surfaces

To improve limited CHF, various surface enhancement techniques have been employed including microporous coating/structures [20,24,31-33], hybrid nano-/micro-structures [16,34], rough surfaces [13,17,26,5,35], nano-coatings [27], and micro-channels/grooves [3,38-40]. The CHF enhancement mechanisms vary, and Hu et al. [118] categorize them into four, i.e., (1) increased departure frequency of coalesced bubble [119], (2) increased three-phase contact line length accompanying increased liquid meniscus formation [120,121], (3) microconvection around the growing and/or coalesced bubbles [122], and (4) heating surface liquid rewetting through radial capillary wicking [9,86,119,120,123-126]. However, the extensive studies have mainly focused on the horizontal upward facing boiling surfaces [44,127-131]. This review focuses on the enhanced CHF using engineered surfaces at different surface orientations as detailed below.

4.1. Surface roughness modification

Deev et al. [132] conducted a PB experiment, which included both nucleate and film boiling regimes, using a square copper boiling surface, 30 mm × 30 mm, and saturated liquid helium as the working fluid. The study was carried out over a range of pressures, 0.445 to $0.98p/p_c$, surface orientations, 0 and 90°, and the average surface roughness of 0.08 and 0.3 μm. They carried out the PB tests under both increasing and decreasing heat flux operations, however, only the nucleate PB under ambient pressure were shown in Fig. 19. They found that the HTC does not vary with the surface orientation, which agrees with those reported

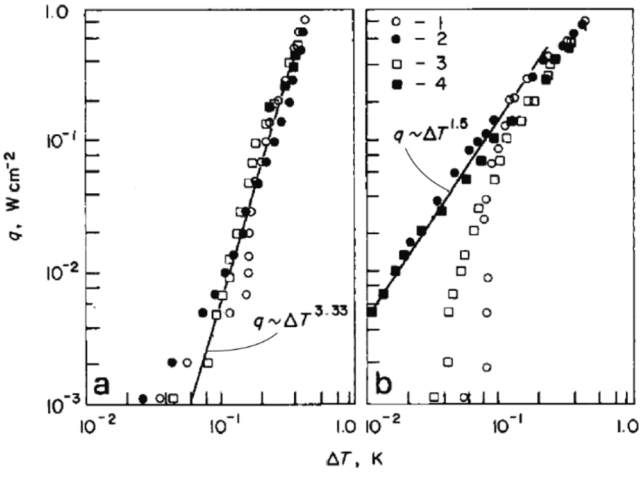

Fig. 19. Nucleate PB for different boiling surface roughness and orientation (a) polished surface – with average roughness of 0.08 μm (b) rough surface – with average roughness of 0.3 μm. The circular symbols represent the horizontal upward surfaces, while the square symbols represent the vertical (90°) surfaces. Moreover, the empty symbols represent increasing heat flux while the solid symbols represent decreasing heat flux [132].

by Lyon [93] and Bewilogua et al. [94].

Nishio and Chandratilleke [133] studied the combined effects of boiling surface roughness and orientation on the nucleate PB using saturated helium at ambient pressure. A solid 20 mm diameter copper rod with the polished surface was used as a boiling surface, and the surface orientations were 0, 45, 90, 135, 157, 175, and 179°. The boiling with a mirror-finished surface was used as a baseline. Only the nucleate PB data for the baseline surface at 0, 90, and 175° surface orientations, were clearly presented by Nishio and Chandratilleke [133] as shown in Fig. 20, and the data show that the HTC increases as the surface

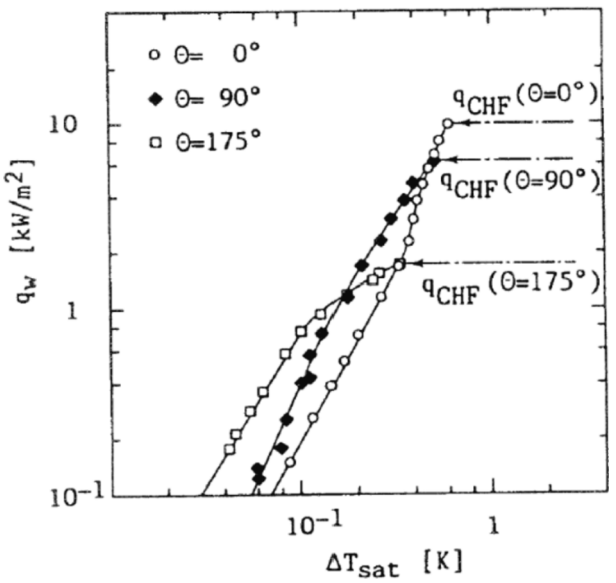

Fig. 20. Effects of surface orientation on nucleate PB heat transfer [133].

orientation increases. The CHF, on the other hand, decreases as the surface orientation increases.

4.2. Microporous coated surfaces

Chang and You [72] have studied the effects of the surface orientation on nucleate PB in saturated FC-72. To account for the horizontal upward-facing, inclined upward-facing, vertical, inclined downward-facing, and horizontal downward-facing orientations, 0, 45, 90, 135, and 180° surface orientations were selected in the experimental study, with degassed distilled water as the working fluid. Two enhanced boiling surfaces, each 10 mm × 10 mm, were tested to compare with the performance of a plain (uncoated) boiling surface serving as a baseline. One surface was coated with copper particles, while the other was coated with aluminium particles. Based on the materials used in the manufacturing process, the former was labelled CBM (Copper Brushable-Ceramic Methyl-ethyl-ketone) and the later labelled ABM (Aluminum Brushable Methyl-ethyl-ketone). In the horizontal upward-facing boiling surface orientation, they reported that both CBM and ABM showed 80% reduction in boiling incipience superheat and about 330 and 100% increase in the nucleate PB heat transfer coefficient and in CHF, respectively, compared to the plain surface. The enhancement is attributed to the increase in nucleation site densities from the surface microstructures, highlighting that the roles of micro-structure on the CHF are omitted in the Zuber theory [110]. A summary of the effect of boiling surface orientation is given as: (a) As shown in Fig. 21(a), the nucleate PB heat transfer coefficient showed the significant enhancement at lower heat flux when the boiling surface inclination changes from 0 to 90°, for the plain surface. The enhancement results from the increase in the number of active nucleation sites, especially in the 90°-oriented (vertical), due to the interaction between the departing bubbles and boiling surface, i.e., the departing bubbles generated from active nucleation sites activate the inactive nucleation sites along their path on the heating surface. A significant HTC decrease was observed when the surface orientation changes from 90 to 180° owing to the increase in the thermal resistance from the elongated bubble and increased bubble departure time. A decreased CHF was also found due to the increased bubble residence time as the boiling surface orientation changes from 0 to 90° as shown in Fig. 21(a). When the heating surface is inclined in downward-facing orientations, i.e., > 90°, most of the generated bubbles coalesce with adjacent ones as they slide along the boiling surface, followed by departing the surface by buoyancy as they approach the tail of the boiling surface. At a surface orientation of 180°, however, the bubbles hover below the heating surface, and the limited bubble escaping pathways result in the bubbles coalesce to form very thick and large bubbles. The coalesced bubbles cover the entire heating surface, serving as a vapor thermal blanket. They concluded that the large vapor thermal blanket in the downward-facing orientation, the CHF is a result of surface dryout rather than hydrodynamic-instability driven CHF. (b) As shown in Fig. 21(b), no significant changes in the HTC and superheat were found regardless of surface orientations as the boiling curves are very similar. The surface orientation independence of the boiling performance is related to the stability in the nucleation site density, i.e., the number of nucleation sites does not change due to the presence of the surface microstructures. On the other hand, the CHF decreases as the surface orientation changes from 0 to 90° due to the increase in the bubble residence time on the heating surface.

Furthermore, the normalized CHF by the CHF at the upward-facing surface for the plain and microstructures shows the similarity as shown Fig. 22, concluding that the CHF mechanism is controlled by the boiling surface orientation relative to the gravitational field.

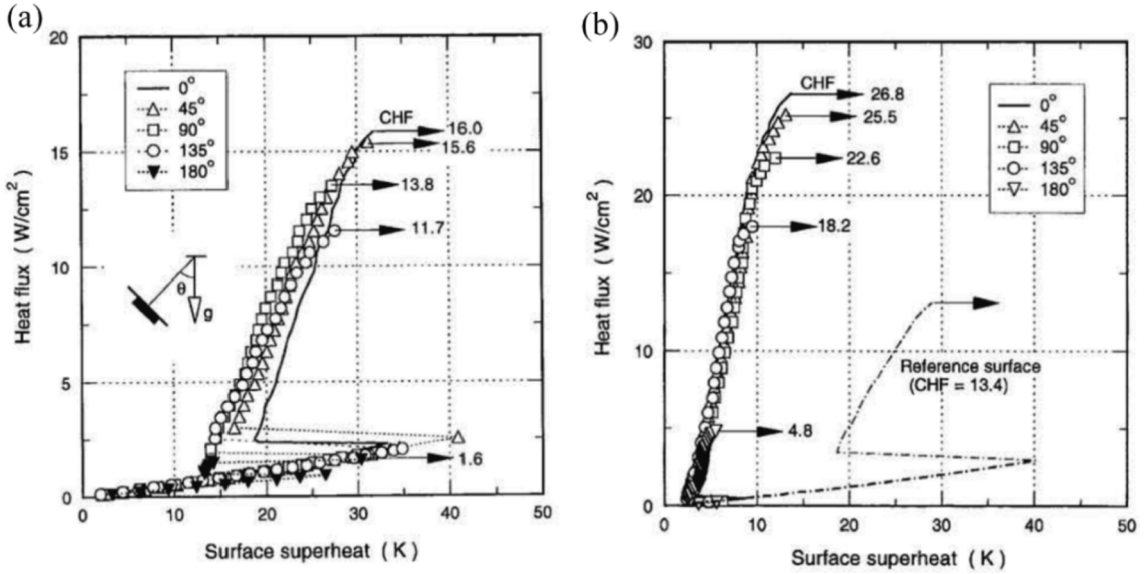

Fig. 21. Nucleate PB curve on (a) plain surface and (b) surface coated with copper particles [72].

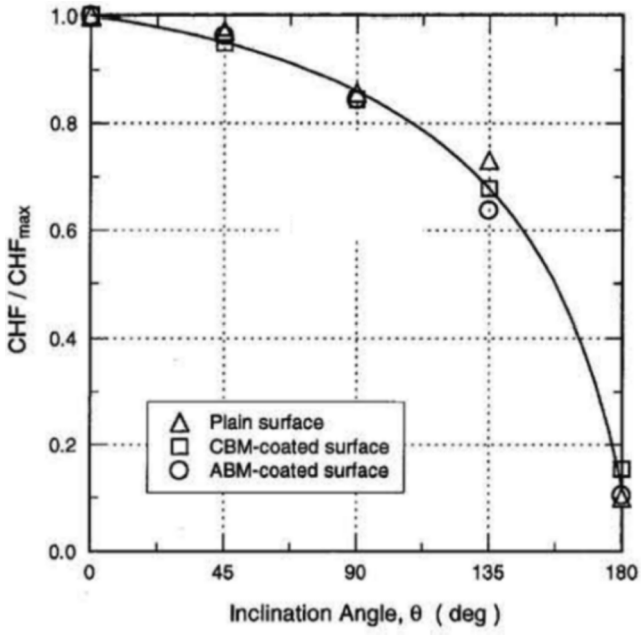

Fig. 22. Normalized CHF as a function of the boiling surface orientation [72].

More recently, Rainey and You [31] developed a CHF correlation for plain and microporous coated surfaces based on the experimental results from 0, 45, 90, 135, 160, and 180° surface orientations on surface sizes of 1, 4, and 25 cm^2, with FC-72 as the working fluid. For the plain surfaces, both CHF and HTC decrease as the surface orientation increases as shown in Fig. 23(a)–(c). They report that these reductions were more pronounced between 135 and 180° due to the increased difficulty of bubble departure by buoyancy force. They also show that the CHF in inclined downward-facing positions is dominated by the surface dryout due to the increased vapor residence time near the boiling surface, while that of inclined upward-facing positions is primarily caused by the hydrodynamic instability.

The microporous coated surfaces do not change the HTC significantly as shown in Fig. 23(a)–(c). This is related to the fact that the larger number of active nucleation sites provided by the microporous surface overshadows other heat transfer enhancement mechanism from the increased surface orientation. On the other hand, the CHF exhibited the same behavior as the plain surfaces, since it gradually decreases as the surface orientation changes from 0 to 135°, and it significantly reduces above 135°. Finally, they demonstrated that the CHF of both the plain and coated microporous boiling surfaces follow a similar trend as the fitted empirically-derived equation of their previous work [72] as shown in Fig. 23(d).

Most recently, Jun et al. [103] presented the boiling surface orientation effects on the nucleate PB heat transfer performance (CHF and HTC) of distilled water at near-saturated condition using two enhanced copper surfaces, each 1 × 1 cm^2 for orientation angles from 0 to 180° with a 45° increment, and then compared with that of a plain copper surface reported by Kwark et al. [134]. The surface enhancements were carried out using sintered copper particles with the average particle size of 67 μm, and the resulting surfaces were referred to as high-temperature thermally conductive microporous coating (HTCMC). The sole difference between the two surfaces is the manufacturing process; the one was sintered in a vacuum environment, while the other was sintered in a nitrogen-filled chamber. The boiling curves for both boiling surfaces at the horizontal upward-facing surface showed that they achieved the same maximum heat flux, approximately 2 MW/m^2, twice that of the bare copper surface, albeit the vacuum sintered surface had higher wall superheat due to its larger solid–liquid contact angle as shown in Fig. 24. They also studied the mechanism that could explained the significant differences between the CHF and HTC for the enhanced and plain surfaces using the visualization technique, and reported that the boiling incipience heat flux is much lower in HTCMC than in plain surface for each surface orientation, however, only visualization images for 0, 90, and 180° surface orientations for the HTCMC sintered in nitrogen and the plain copper surfaces were presented as shown in Fig. 25.

Fig. 26 shows the CHF for all the surfaces increased slightly as the surface orientation increases from 0 to 90° for all the boiling surfaces, which do not agree to other work in literature [87,94,133,72,31]. Furthermore, the CHF for both enhanced surfaces were reported to be similar at each surface orientation, and the surface enhancements increased the CHF by 1 MW/m^2 relative to the plain surface at each surface orientation. Between 90 and 170°, the CHF decreased marginally as the surface orientation increased, and beyond 170° a sharp decrease in CHF was observed. As Howard and Mudawar [57] have similarly done, Jun et al. [103] classified the boiling curves into three regions [A, B, and C as shown in Fig. 26(a) and (b)] with respect to the behavior of the CHF with the surface orientation, and also reported a transition angle of 170° which agree to the previous studies.

Borumand and Hwang [135] modified the original interfacial lift-off model by Howard and Mudawar [57] to study pool boiling CHF enhancement on near-vertical surfaces ($\theta = 60°–130°$) using columnar-post wicks. The study showed that for water at the small columnar-post pitch distances (< 2.5 mm) CHF increases from 104 to 295 W/cm^2 for $\theta = 90°$, and from 89 to 313 W/cm^2 for $\theta = 120°$, i.e., 185 and 250% enhancement, respectively, compared to the plain surface. The enhancement results from the tailored hydrodynamic-instability through engineered wetting fronts using columnar-post wick.

4.3. Other surface enhancements

Jung et al. [136] investigated the combined effects of boiling surface enhancement and orientation on both nucleate and film boiling heat transfer using R-11 as a working fluid. The boiling surface was a flat circular disk with a dimeter of 78 mm for two enhanced boiling surfaces, UNB#1 and UNB#2. The obtained experimental results were compared with a plain surface. The enhanced surfaces were made by surface deposition of metal particles on plain mild steel plates, while the plain copper disk was prepared by polishing with a coarse emery paper. The surface orientations were 0, 45, 90, 135, 150, 165, 170, and 180°, and the boiling chamber was kept at 2 bar for each boiling surface-type and orientation.

They pointed out that the knees on the boiling curves show the existence of incipient boiling points, stating that any small increment in heat flux beyond the minimum superheat required for incipient boiling led to vigorous boiling that is accompanied with a sudden drop of the boiling surface temperature. They further noted that at high heat flux, the nucleate boiling is similar regardless of surface orientation as shown in Fig. 27(a)–(c). This indicates the similar HTC are associated with the similar number of active nucleation sites on the boiling surface at high heat flux.

The surface orientation effects on nucleate boiling heat transfer for the plain copper surface and UNB#2 surface are shown in Fig. 28, including the part of the film boiling regime. They reported that, for all the surfaces, the wall superheat decreased by 15–25% as the boiling surface orientation changed from 0 to 165° in the nucleate boiling regime at the heat flux range of 10–40 kW/m^2. Beyond this range of heat flux, they found that the surface superheat remained constant regardless of the surface orientation, except in the downward-facing case, where the stratification of vapor bubbles on the underside of the boiling surface resulted in significant increase in the surface superheat, as shown in Fig. 28(a) and (b). Based on visual observations, they concluded that at least two types of heat transfer mechanism are associated with nucleate boiling for the inclined surfaces: (a) the evaporative mechanism is independent of the surface orientation and controlled by the input heat flux, and (b) the bubble agitation mechanism that has a strong

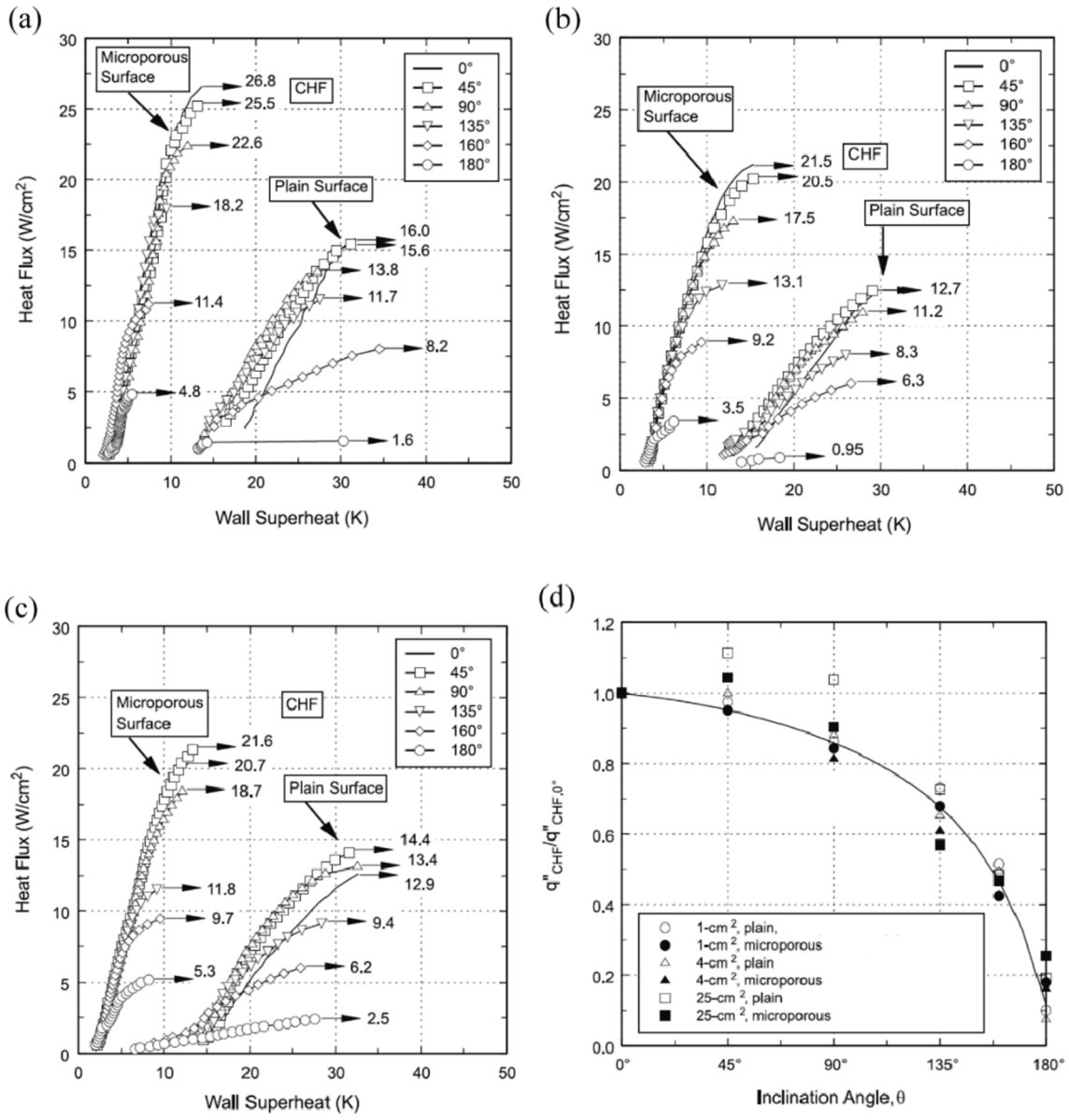

Fig. 23. (a) Heat flux as a function of wall superheat for 1 cm^2 surface at different surface orientations, (b) heat flux as a function of wall superheat for 4 cm^2 surface at different surface orientations, (c) heat flux as a function of wall superheat for 25 cm^2 surface at different surface orientations, and (d) normalized CHF data as a function of surface orientations [31].

connection with the surface orientation. They reported that for inclined boiling surfaces, the first mechanism was dominant at high heat fluxes, while the second mechanism, which is initiated by bubble flow over the boiling surface, was dominant at low heat fluxes.

Reed and Mudawar [112] also reported that the CHF decreases as the surface orientation increases from the upward-facing to downward-facing, when they studied the boiling heat transfer enhancement using FC-72 and FC-87 with pressed-on fins at low contact forces as shown in Fig. 29. The experimental results also showed that the nucleate PB HTC is independent of the surface orientation with respect to gravity at high heat flux.

Kim and Suh [137] considered the combined effects of surface orientation and the gap size (or confinement) on CHF during the nucleate PB of water at ambient pressure with a one-dimensional heating surface confined in a rectangular channel. The boiling surface was a 15 mm × 15 mm rectangular copper surface, coated with the thin film of nickel to prevent oxidation. The water pool was kept at saturated condition, for different surface orientations from 90° to 180° and confinement sizes of 1, 2, 5, and 10 mm. The testing facility consisted of the boiling surface-orientation converter unit, a reflux condenser, an auxiliary immersion heater, vacuum pumping system, thermocouples, and a data acquisition unit, as shown in Fig. 30.

As shown in Fig. 31, it was found that the CHF decreases as the surface orientation increases from 90 to 180° for each confinement size, which are reasonably consistent with the previous work by Monde et al. [138]. Similar to Yang et al. [68], Howard and Mudawar [57], and Jun et al. [103] using unconfined heating surface, they reported the transition angle of 65, 170, and 175° for the gap size of 2, 5, and 10 mm, respectively.

Liao et al. [117] observed the coupling effects of the surface orientation and solid–liquid contact angle on the heat transfer and CHF nucleate PB of saturated water at ambient pressure. Three different 20-mm-diameter copper surfaces, each with different surface contact angles, were employed in the PB experiment. The surface orientation angles were 55° (plain surface), 30° (surface A) and 0° (surface B), where the surface enhancements to promote wettability were achieved using

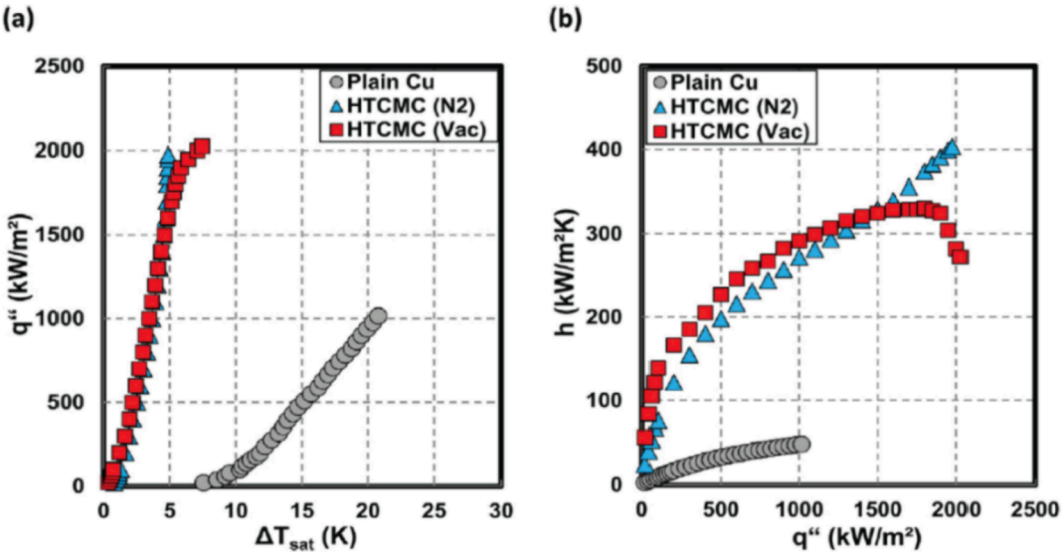

Fig. 24. (a) Boiling curves for the HTCMC and the plain copper surface (b) heat transfer coefficient for the HTCMC and the plain copper surface. Note that these results are for the horizontal upward-facing orientation [103].

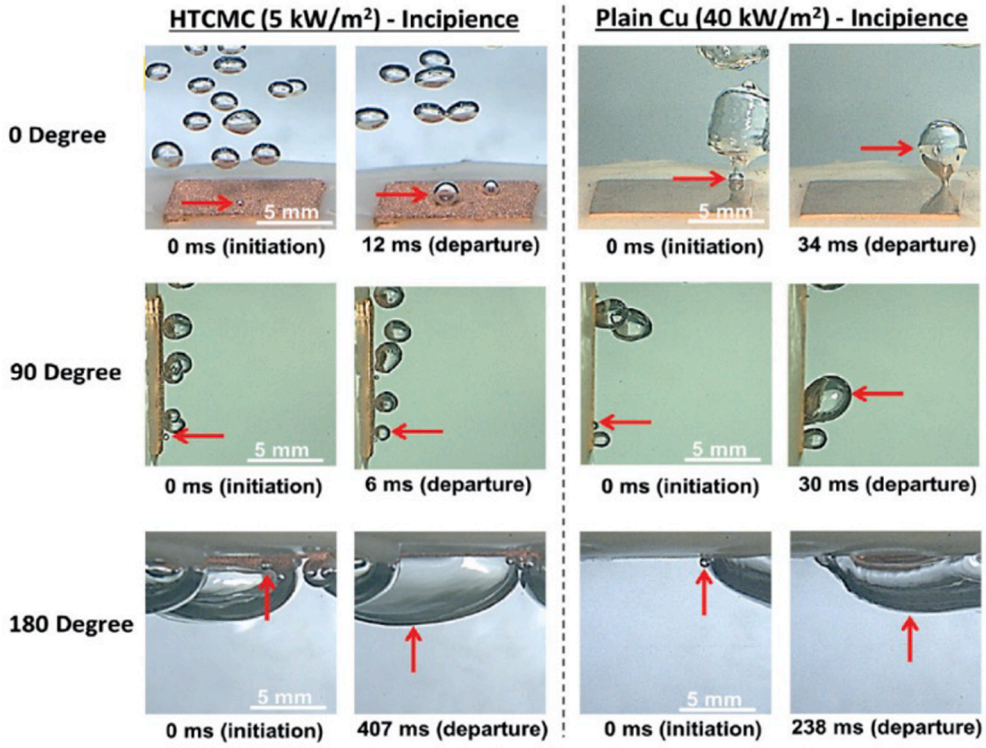

Fig. 25. Comparison of the boiling incipience of the nitrogen-sintered HTCMC and plain copper surfaces at surface orientations of 0, 90, and 180° [103].

TiO_2 coatings. The surface orientations were between 0 and 180° at 45° intervals. They reported that the HTC of surface A was marginally smaller than the plain surface, while that of surface B was substantially smaller, attributing to the decreased HTC as the contact angle decreases to the reduction in the number of nucleation sites. This result supports the previous studies that the hydrophobicity promotes the formation of nucleation sites. They made three main conclusions. (a) For the plain surface, there was no significant change in the CHF when the surface orientation changes from the upward facing to vertical position due to the easy bubble escape from the surface. However, beyond 90°, the CHF decreases drastically as the surface orientation increases due to the early initiation of boiling crisis by the coalescing and accumulating vapor bubbles on the heating surface, with the CHF at 135 and 180° decreasing by 14 and 76%, respectively. (b) The HTC for the plain surface decreases marginally as the surface orientation increases from 0 to 90° but decreases dramatically as it increases beyond 90°. The dramatic decrease in HTC is primarily due to the thermal insulation by the trapped thick vapor layer underneath the downward-facing surfaces. (c) The CHF for surfaces A and B showed the similar behavior to the plain surface as the surface orientation changes from 0 to 90°, however, the CHF increases for surface A relative to the plain surface at surface orientation between 0 and 180° was between 7 and 12% while that of surface B was between 16 and 28%, showing the significant and complex effect of solid–liquid contact angle on CHF as shown in Fig. 32.

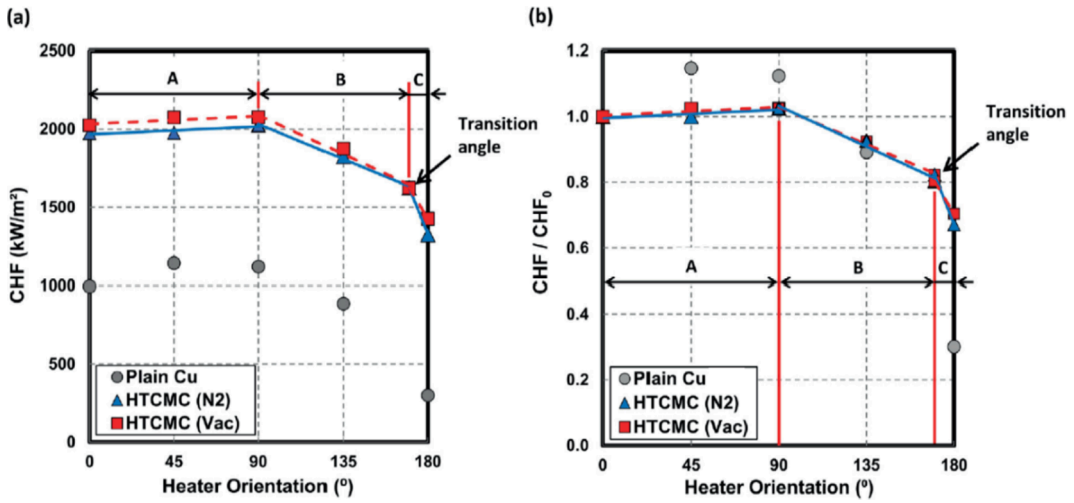

Fig. 26. (a) CHF data for the HTCMC and plain copper surface at the various orientation angles. (b) Normalized CHF data for the HTCMC and plain copper surface, A. upward-facing to vertical (0 − 90°), B. vertical to inclined downward-facing (90 − 170°), and C, inclined downward-facing to downward-facing (170 − 180°) [103].

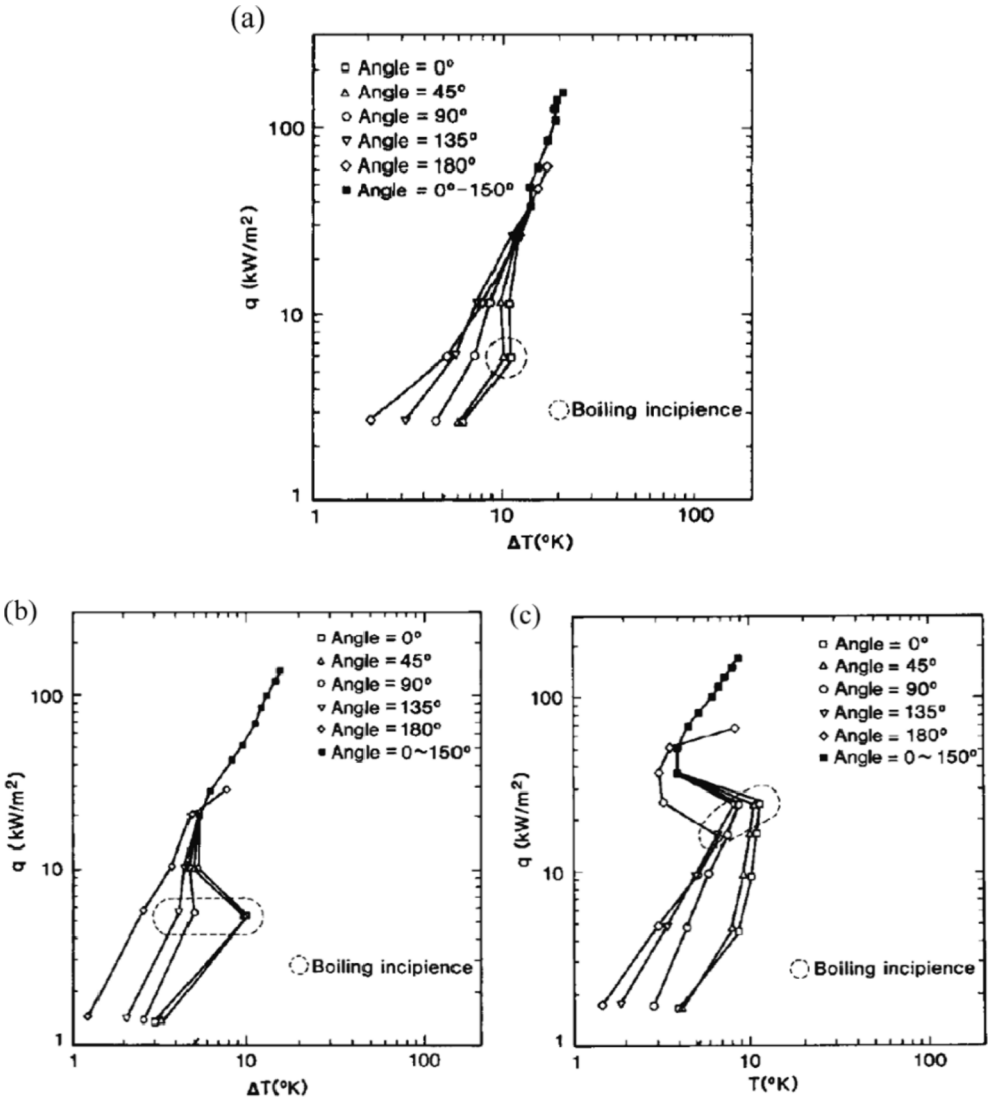

Fig. 27. Heat flux versus wall superheat for the (a) plain copper surface, (b) UNB#1, and (c) UNB#2 surfaces [136].

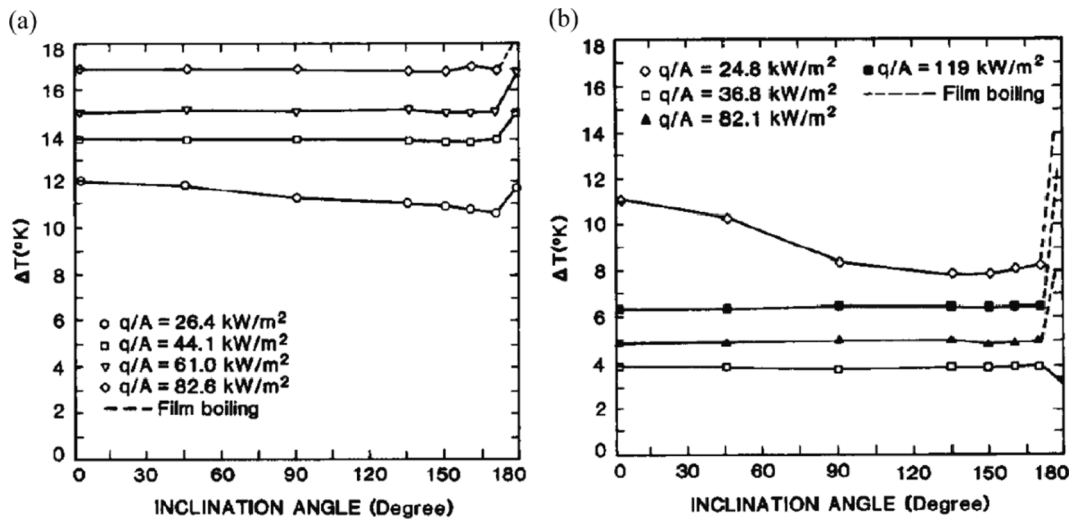

Fig. 28. (a) Wall superheat as a function of surface orientation at different heat fluxes for the plain copper surface, (b) wall superheat as a function of surface orientation at different selected heat fluxes for the UNB#2 surface [136].

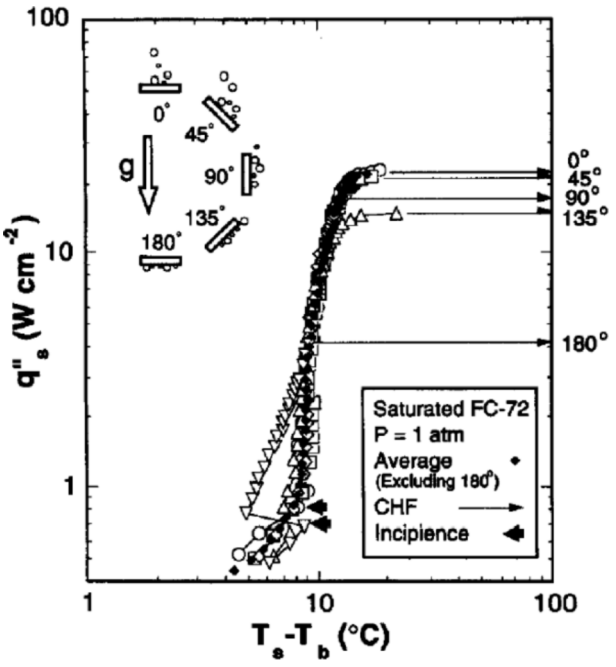

Fig. 29. Heat flux as a function of wall superheat for different surface orientations [112].

More recently, Narayan et al. [139] examined the effect of surface orientation on PB heat transfer of nanoparticles suspension using a smooth (48 nm in average surface roughness) tubular boiling surface, 33 mm and 170 mm in diameter and length, respectively. The nanofluid was an electrostatically stabilized water-based nanoparticles suspension containing aluminum oxide (alumina) nanoparticles. Three different nanoparticle concentrations, 0.25, 1, and 2 wt%, were tested at surface orientations of 0, 45, and 90°. The test setup used was made up of a boiling vessel, 12 cm × 12 cm × 30 cm in dimension, a condenser with cooling water circulation system, and a regulated auto-transformer power supply, as shown in Fig. 33. Secondary heaters were also employed for preheating and degassing the boiling liquid and to maintain the boiling liquid at saturated liquid.

Fig. 34 shows that for water-alumina nanoparticle (average particle size of 47 nm) suspension of 2 wt% concentration, the surface orientations of 0° achieved higher heat transfer coefficient (HTC) compared to the vertical and 45°-oriented surface. However, the HTC difference from the different surface orientations decreases as the heat flux increases. A similar trend was observed with other nanofluid concentrations, i.e., 0.25 and 1 wt%. Note that the HTC enhancement with the 0.25 wt% nanoparticle concentration was moderate compared to no nanoparticles, while the higher nanoparticle concentration decreases the HTC as the deposition of the nanofluid particles on the boiling surface reduces the active nucleation sites.

Nanoparticles are known to be deposited on the boiling surface during PB of nanofluids, and the rate of deposition depends on the concentration of the nanofluid [25,140-147]. This surface deposition promotes the deactivation of nucleation sites, undermining heat transfer effectiveness [143,148]. In the case of the horizontal tube, nucleation was found to occur mainly on the underside of the tube, and since, in general, the rate of nanoparticle deposition on the underside of a downward-facing surface is very low by virtue of the forces involved in particle deposition, the number of deactivated nucleation sites is lower when the tube is at 0° compared to the inclined surface. Furthermore, to verify the reason for the modified bubble sliding motion on the inclined heating surface, the range of the temperature decrease between the top and bottom of the heat transfer tube when inclined at 45° were measured, both for the base fluid (water) and the nanofluid. That of the base fluid was between 1.3 and 2.3 K, while that of the nanofluid was between −0.2 and 1.2 K, and they claimed that the difference was a result of the impedance offered to the sliding bubbles by the nanoparticles close to the heating surface on inclined surface.

Most recently, Kwark et al. [134] studied the combined effects of pool pressure, surface orientation, and the geometric size on nucleate PB of water with nano-coated boiling surfaces. The performance of the nano-coated surfaces was also compared with that of a plain surface to enhance both CHF and HTC. Although three different nano-particle sizes (79, 139, and 210 nm) and four different surface areas (56.25, 100, 225, 400 mm^2) were used to study the effects of particle size, pool-chamber pressure, and surface orientation, only the 100 mm^2 surface coated with 139 nm particles was used to investigate the effects of surface orientation. The boiling curves for both nanocoated and plain surfaces, at different surface orientation are shown in Fig. 35. At heat fluxes below 100 kW/m^2, the HTC increases with the surface orientation, however, at higher heat fluxes (>100 kW/m^2), the HTC is similar regardless of the surface orientation, which agree to previous studies. Lienhard [149] explained that the reason could be due to the transition from the isolated bubbles regime, where there is a time gap between successive departing

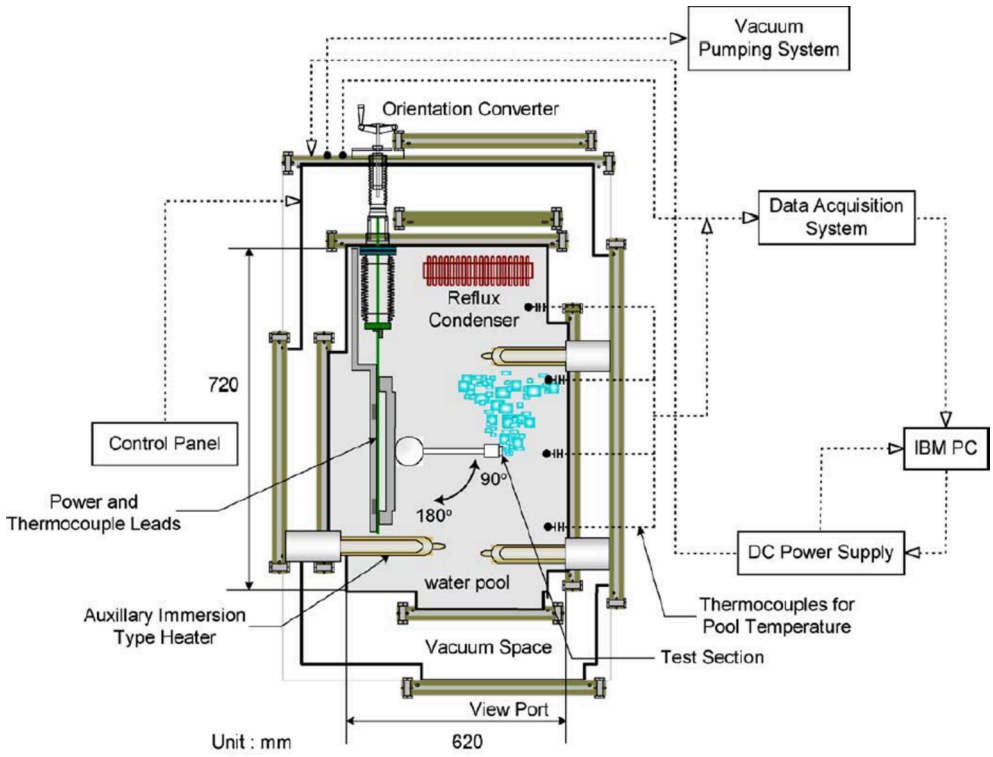

Fig. 30. Schematic of the experimental facility used in the study of the effect of surface orientation and gap size on CHF [137].

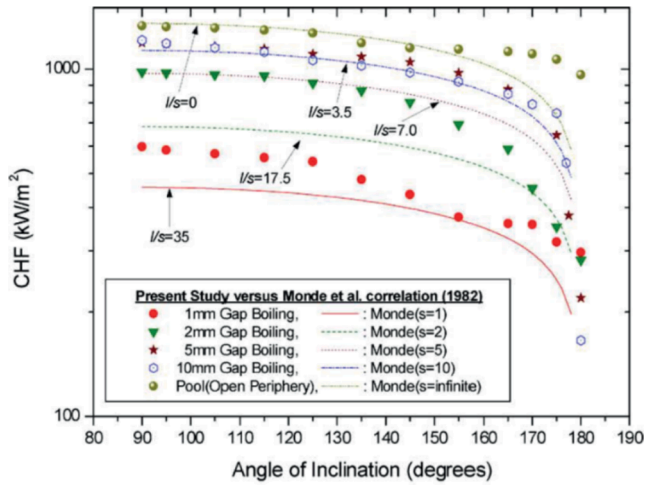

Fig. 31. CHF as a function of the surface orientation for different heater length, l to channel gap size, s, ratio, l/s. [137]

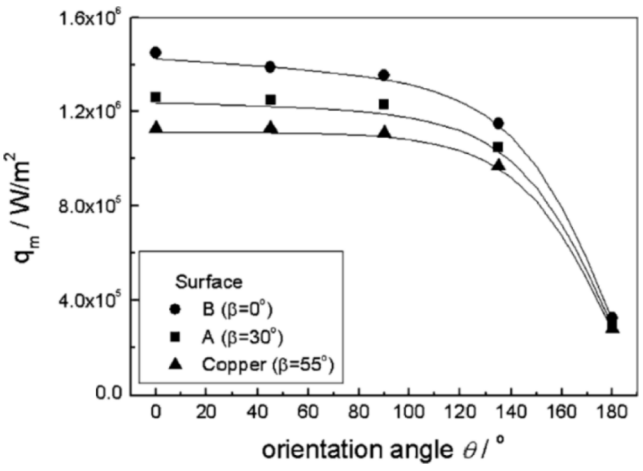

Fig. 32. The CHF for the plain copper surface, surface A, and surface B. Note that β is the solid–liquid apparent contact angle [117].

bubbles, to the continuous vapor column regime, where boiling is vigorous and the rate of bubble departure is very high which leaves successive departing bubbles to form travelling columnar vapor packs.

Fig. 35 also shows that the reduction in CHF between 0 and 90° for both the uncoated and nanocoated surfaces was marginal, but very dramatic beyond surface orientation of 90°. Kwark et al. [134] also attributed the dramatic decrease in CHF to the increase in the bubble residence time on the boiling surface. As previously mentioned, the bubbles on downward-facing surfaces cannot detach freely by buoyancy, and as a result, they flatten as they grow, merging with adjacent ones as they slide along the heated surface. The time required for the entire boiling surface to cover in a vapor blanket is dependent on the surface orientation, the heat flux, the surface wettability, and the pressure within the pool-chamber. The combined effect of boiling chamber pressure and boiling surface orientation on PB performance is yet to be investigated extensively.

4.4. Summary

The studies on engineered surfaces with surface orientations CHF and HTC for the PB surface orientation are summarized in the following. (1) The majority of the studies focused on the effect of surface orientation on the CHF, and these studies showed that CHF slightly decreases with surface orientation between the horizontal upward facing, i.e., 0° and vertical orientation, i.e., 90°, but dramatically reduces between 90° and horizontal downward facing, i.e., 180°. (2) Various surface enhancement techniques significantly increases the PB CHF with little or no effect on the HTC. The improvement in CHF is related to the (a) increased departure frequency of coalesced bubble, (b) increased three-

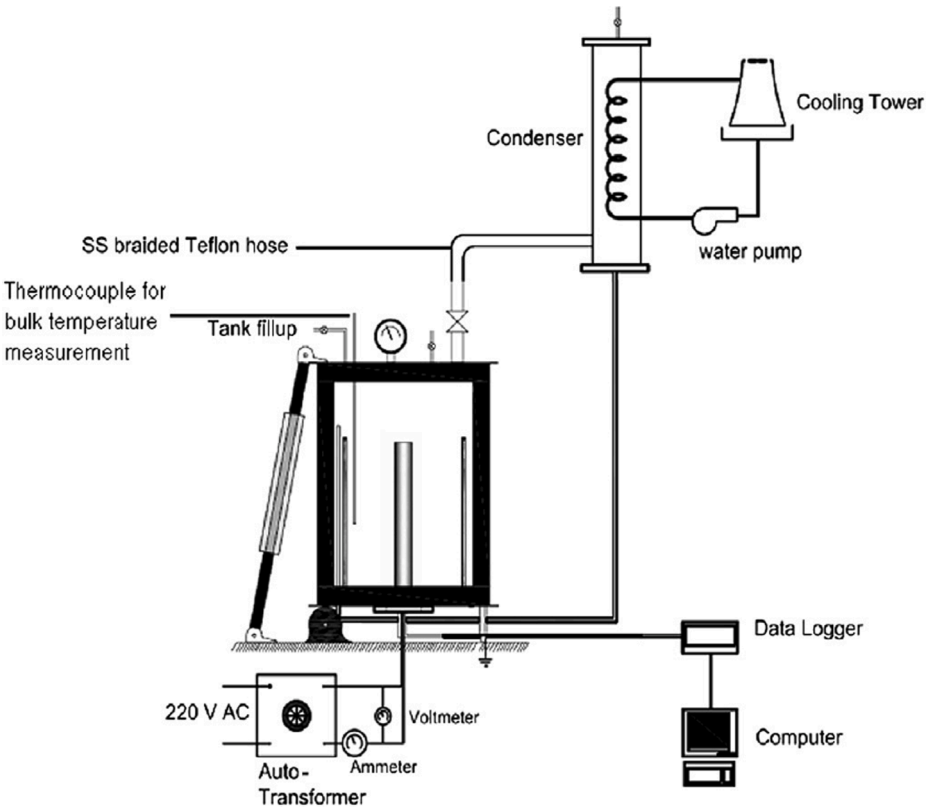

Fig. 33. The experimental setup used in the study of the effect of surface inclination and concentration of nanofluid on the CHF and HTC [139].

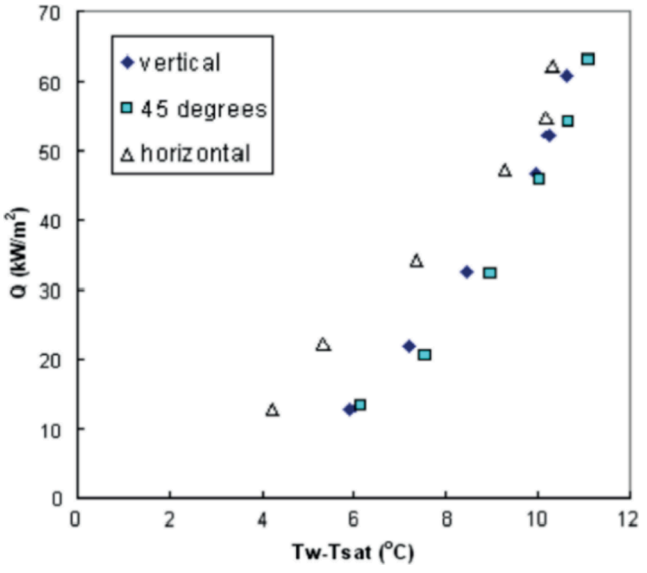

Fig. 34. Heat flux as a function of wall superheat for the surface orientation of 0, 45, and 90°. water-alumina nanoparticles – 2 wt%, 47 nm particle [139].

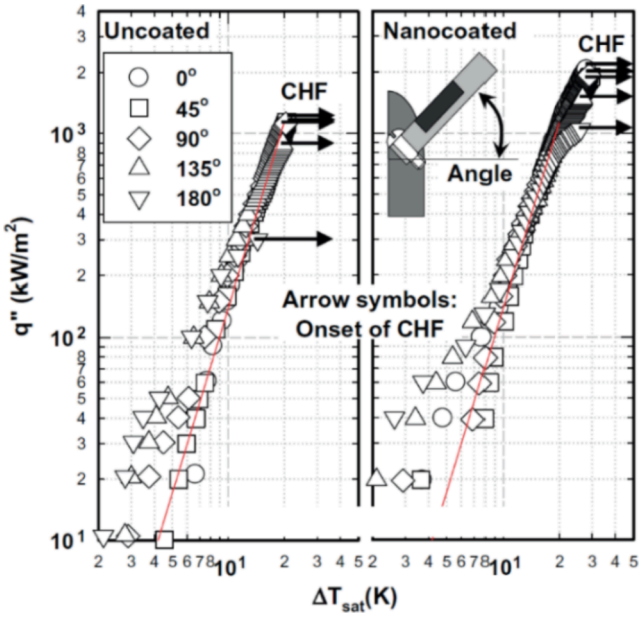

Fig. 35. Heat flux as a function superheat for the uncoated and nanocoated heater surfaces [134].

phase contact line length accompanying increased liquid meniscus formation, (c) microconvection around the growing and/or coalesced bubbles, (d) heating surface liquid rewetting through radial capillary wicking, and (e) effective and efficient separation of unwanted vapor from the liquid supply.

5. Conclusion

The nucleate pool-boiling heat transfer is identified as one of the promising two-phase thermal management systems for various applications including the electronics, transportation, microfluidics, biomedical engineering, metallurgical industry, refrigeration, energy conversion, and space exploration systems. The nucleate PB heat transfer has been extensively studied on the upward facing surface, i.e., 0°, but the study on the larger surface orientations, i.e., 0° to 180°, has been limited, although understandings of HTC and CHF are crucial to

optimally design and operate thermal management systems in the large surface orientations. From the extensive literature reviews on the effects of surface orientations on nucleate PB heat transfer, the following conclusions are drawn:

- At pre-CHF, the HTC increases as the surface orientation increases from the upward facing to the vertical surfaces, i.e., 0 to 90°, attributing to the increased active nucleation sites.
- For the plain boiling surfaces, the CHF decreases marginally as the surface orientation increases from the upward-facing to near-downward surface, i.e., 90° to 165°. This moderate reduction is related to the bubble escape process is sluggish by the inefficient bubble growth/sliding mechanisms on such a large surface orientation. At the large surface orientation, i.e., > 165°, the CHF significantly decreases, because the generated bubbles are stratified over the heating surface, followed by eventually forming a thermal vapor blanket.
- The effect of surface orientation on CHF and HTC of nucleate PB is independent of the type of working fluid and based on the analysis of the capture images of the liquid–vapor-heating surface interactions and dynamics the boiling process can be divided into three: (1) horizontal upward-facing, (2) near-vertical, and (c) downward-facing, each of which have different physical CHF triggering mechanisms. The CHF slightly decreases as the boiling surface orientation increases from the horizontal upward facing (0°) to the vertical position (90°) and then decreases rapidly beyond 90°, except in the work of Jun et al. [103] who found that the CHF increased slightly between 0 and 90° before rapidly decreases towards the horizontal; downward facing (180°).
- The HTC and CHF reduce due to the poor vapor escape mechanisms from the surface at > 90°, i.e., sluggish bubble sliding behavior. However, the study on the enhanced surface for the large surface orientation is limited. The novel engineered surface is needed to offer the enhanced HTC and CHF by efficiently separating the unwanted vapor layer from the liquid supply.
- The correlation for the HTC of different surface orientations is very limited, i.e., only the modified wall boiling model with the observed bubble generation/coalesce density to predict the plain surface. Extensive studies for the different surface conditions such as different types of materials, wetting, microstructures, etc. are crucial to improve the predictive tools for the nucleate PB system designs and operations.

6. Future research directions

Despite extensive studies, there are a few contentious discussions on the tailored two-phase flow via the surface orientations and their relations to HTC reduction and CHF triggering mechanisms. The poor understandings are mainly related to the lack of (a) consistent study result data base systems, (b) required two-phase flow visualization study, and (c) tailored two-phase flow mechanisms. To articulate aforementioned tailored two-phase flow with the surface orientations and their relations to the HTC and CHF, the following future research is suggested:

- The consistent pool boiling experiment data base systems are critically needed as the previous studies have used different heating surface material composition, size, morphology, surface orientation, and working liquid. The future studies require to conduct the pool boiling experiments for the surface orientations, while keeping other experimental conditions the same, focusing on the effects of heating surface orientation on HTC and CHF.
- Current two-phase flow visualization tools do not capture the fast-two-phase flow dynamics with the required images qualities, especially near the heating surface. The development of innovative two-phase flow visualization techniques for real-time, fast two-phase flow dynamics is critically needed.
- The CHF triggering mechanisms on upward facing surface orientation are still under contentious discussions such as hydrodynamic-instability-, surface-wetting-, or capillary-flow-driven-liquid chocking, etc, and similarly on the different surface orientations where the buoyancy flow direction is different. The CHF triggering mechanisms on the different surface orientations can be examining using various engineered surfaces including micro-/nanostructured and wetting surfaces. Such fundamental understandings will provide insights into the optimal surface designs of enhanced boiling heat transfer.
- Recent studies have employed superhydrophilic, superhydrophobic, biphilic (i.e., hydrophilic-hydrophobic or superhydrophilic-superhydrophobic) boiling surfaces [11,7,150-153], most of which were manufactured using chemical processes, in PB heat transfer experiments. However, these surfaces have been tested in upward facing orientation, i.e., 0°, thus it would be interesting to examine the effect of surface orientation on these surfaces since the two-phase flow dynamics in these surfaces have been found to be very different from surfaces with enhanced wettability achieved through conventional surface modifications such as micro-indentation, i.e., increased roughness, and coating.

Declaration of Competing Interest

The authors declare that they have no known competing financial interests or personal relationships that could have appeared to influence the work reported in this paper.

Acknowledgements

This work is financially supported by NASA Cooperative Agreement Notice, Grant Number 80NSSC18M0030, the National Science Foundation (NSF), Award No. OIA-1929187, and the Wichita State University Convergence Sciences Initiative Program, and the College of Engineering, Department of Mechanical Engineering, Wichita State University.

References

[1] V.M. Wasekar, R.M. Manglik, A review of enhanced heat transfer in nucleate pool boiling of aqueous surfactant and polymeric solutions, J. Enhanc. Heat Transf. 6 (2–4) (1999).
[2] J. Barber, D. Brutin, L. Tadrist, A review on boiling heat transfer enhancement with nanofluids, Nanoscale Res. Lett. 6 (1) (2011) 280.
[3] J.R. Thome, Boiling in microchannels: a review of experiment and theory, Int. J. Heat Fluid Flow 25 (2) (2004) 128–139.
[4] M. Shoji, Studies of boiling chaos: a review, Int. J. Heat Mass Transf. 47 (6–7) (2004) 1105–1128.
[5] I.L. Pioro, W. Rohsenow, S.S. Doerffer, Nucleate pool-boiling heat transfer. I: review of parametric effects of boiling surface, Int. J. Heat Mass Transf. 47 (23) (2004) 5033–5044.
[6] G.R. Warrier, V.K. Dhir, Heat transfer and wall heat flux partitioning during subcooled flow nucleate boiling—a review, 2006.
[7] H. Jo, H.S. Ahn, S. Kang, M.H. Kim, A study of nucleate boiling heat transfer on hydrophilic, hydrophobic and heterogeneous wetting surfaces, Int. J. Heat Mass Transf. 54 (25–26) (2011) 5643–5652.
[8] J. Kim, Review of nucleate pool boiling bubble heat transfer mechanisms, Int. J. Multiph. Flow 35 (12) (2009) 1067–1076.
[9] H. Kim, Enhancement of critical heat flux in nucleate boiling of nanofluids: a state-of-art review, Nanoscale Res. Lett. 6 (1) (2011) 415.
[10] M. Jamialahmadi, H. Müller-Steinhagen, Scale formation during nucleate boiling-A review, De Gruyter, 1993.
[11] A.R. Betz, J. Jenkins, D. Attinger, Boiling heat transfer on superhydrophilic, superhydrophobic, and superbiphilic surfaces, Int. J. Heat Mass Transf. 57 (2) (2013) 733–741.
[12] J.Y. Chang, S.M. You, Boiling heat transfer phenomena from microporous and porous surfaces in saturated FC-72, Int. J. Heat Mass Transf. 40 (18) (1997) 4437–4447.
[13] J.P. McHale, S.V. Garimella, Bubble nucleation characteristics in pool boiling of a wetting liquid on smooth and rough surfaces, Int. J. Multiph. Flow 36 (4) (2010) 249–260.
[14] J.A. Weibel, A.S. Kousalya, T.S. Fisher, S.V. Garimella, Characterization and nanostructured enhancement of boiling incipience in capillary-fed, ultra-thin sintered powder wicks, in: Thermal and Thermomechanical Phenomena in

Electronic Systems (ITherm), 2012 13th IEEE Intersociety Conference on, 2012, pp. 119–129.
[15] A.R. Betz, J. Xu, H. Qiu, D. Attinger, Do surfaces with mixed hydrophilic and hydrophobic areas enhance pool boiling? Appl. Phys. Lett. 97 (14) (2010), 141909.
[16] S.M. You, J.H. Kim, K.H. Kim, Effect of nanoparticles on critical heat flux of water in pool boiling heat transfer, Appl. Phys. Lett. 83 (16) (2003) 3374–3376.
[17] M.-G. Kang, Effect of surface roughness on pool boiling heat transfer, Int. J. Heat Mass Transf. 43 (22) (2000) 4073–4085.
[18] C. Coyle, H. O'Hanley, B. Phillips, J. Buongiorno, T. McKrell, Effects of hydrophobic surface patterning on boiling heat transfer and critical heat flux of water at atmospheric pressure. ASME 2013 Power Conference, 2013 p. V002T11A005-V002T11A005.
[19] H. Honda, J.J. Wei, Enhanced boiling heat transfer from electronic components by use of surface microstructures, Exp. Therm. Fluid Sci. 28 (2–3) (2004) 159–169.
[20] J.Y. Chang, S.M. You, Enhanced boiling heat transfer from microporous surfaces: effects of a coating composition and method, Int. J. Heat Mass Transf. 40 (18) (1997) 4449–4460.
[21] X. Dai, et al., Enhanced nucleate boiling on horizontal hydrophobic-hydrophilic carbon nanotube coatings, Appl. Phys. Lett. 102 (16) (2013), 161605.
[22] A.S. Moita, E. Teodori, A.L.N. Moreira, Enhancement of pool boiling heat transfer by surface micro-structuring, J. Phys.: Conf. Ser. 395 (2012), 012175.
[23] R.J. Benjamin, A.R. Balakrishnan, Nucleation site density in pool boiling of saturated pure liquids: effect of surface microroughness and surface and liquid physical properties, Exp. Therm. Fluid Sci. 15 (1) (1997) 32–42.
[24] C. Li, G.P. Peterson, Parametric study of pool boiling on horizontal highly conductive microporous coated surfaces, J. Heat Transf. 129 (11) (2007) 1465–1475.
[25] M. Chopkar, A.K. Das, I. Manna, P.K. Das, Pool boiling heat transfer characteristics of ZrO2–water nanofluids from a flat surface in a pool, Heat Mass Transf. 44 (8) (2008) 999–1004.
[26] B.J. Jones, J.P. McHale, S.V. Garimella, The influence of surface roughness on nucleate pool boiling heat transfer, J. Heat Transf. 131 (12) (2009), 121009.
[27] H.T. Phan, N. Caney, P. Marty, S. Colasson, J. Gavillet, Surface wettability control by nanocoating: the effects on pool boiling heat transfer and nucleation mechanism, Int. J. Heat Mass Transf. 52 (23–24) (2009) 5459–5471.
[28] N. Zuber, "Hydrodynamic aspects of boiling heat transfer (thesis)", Ramo-Wooldridge Corp., Los Angeles, CA (United States); Univ. California (1959).
[29] S.G. Kandlikar, A theoretical model to predict pool boiling CHF incorporating effects of contact angle and orientation, J. Heat Transf. 123 (6) (2001) 1071–1079.
[30] D. Attinger, et al., Surface engineering for phase change heat transfer: A review, MRS Energy Sustain 1 (2014).
[31] K.N. Rainey, S.M. You, Effects of heater size and orientation on pool boiling heat transfer from microporous coated surfaces, Int. J. Heat Mass Transf. 44 (14) (2001) 2589–2599.
[32] K.N. Rainey, S.M. You, Pool boiling heat transfer from plain and microporous, square pin-finned surfaces in saturated FC-72, J. Heat Transf. 122 (3) (2000) 509–516.
[33] C.M. Patil, S.G. Kandlikar, Pool boiling enhancement through microporous coatings selectively electrodeposited on fin tops of open microchannels, Int. J. Heat Mass Transf. 79 (2014) 816–828.
[34] H.S. Ahn, V. Sathyamurthi, D. Banerjee, Pool boiling experiments on a nano-structured surface, IEEE Trans. Compon. Packag. Technol. 32 (1) (2009) 156–165.
[35] R.J. Benjamin, A.R. Balakrishnan, Nucleate pool boiling heat transfer of pure liquids at low to moderate heat fluxes, Int. J. Heat Mass Transf. 39 (12) (1996) 2495–2504.
[36] A. Ijaola, K. Arifa, E. Jurak, H. Misak, R. Asmatulu, Effects of acid treatments on physical properties of CNT wires for wiring applications, Nano-, Bio- Info-Tech Sensors 3D Syst. IV 11378 (2020) 113780C.
[37] A.O. Ijaola, R. Asmatulu, K. Arifa, Metal-graphene nano-composites with enhanced mechanical properties, in: Behavior and Mechanics of Multifunctional Materials IX, 2020, vol. 11377, p. 113771E.
[38] D.A. Cooke, S.G. Kandlikar, Effect of open microchannel geometry on pool boiling enhancement, 2012. doi: 10.1016/j.ijheatmasstransfer.2011.10.010.
[39] D. Cooke, S.G. Kandlikar, Pool boiling heat transfer and bubble dynamics over plain and enhanced microchannels, in: ASME 2010 8th International Conference on Nanochannels, Microchannels, and Minichannels collocated with 3rd Joint US-European Fluids Engineering Summer Meeting, 2010, pp. 163–172.
[40] S.G. Kandlikar, Heat transfer mechanisms during flow boiling in microchannels, in: ASME 2003 1st International Conference on Microchannels and Minichannels, 2003, pp. 33–46.
[41] V.K. Dhir, Boiling heat transfer, Annu. Rev. Fluid Mech. 30 (1) (1998) 365–401.
[42] C.H. Wang, V.K. Dhir, Effect of surface wettability on active nucleation site density during pool boiling of water on a vertical surface, 1993.
[43] C.H. Wang, V.K. Dhir, On the gas entrapment and nucleation site density during pool boiling of saturated water, 1993.
[44] G. Liang, I. Mudawar, Review of pool boiling enhancement by surface modification, Int. J. Heat Mass Transf. 128 (2019) 892–933.
[45] I. Malavasi, E. Teodori, A.S. Moita, A.L. Moreira, M. Marengo, Wettability effect on pool boiling: a review, in: Encycl. Two-Phase Heat Transf. Flow III Macro Micro Flow Boil. Numer. Model. Fundam. Vol. 4 Spec. Boil. Top., pp. 1–61, 2018.
[46] F.P. Incropera, A.S. Lavine, T.L. Bergman, D.P. DeWitt, Fundamentals of heat and mass transfer, Wiley, 2007.
[47] E.R.G. Eckert, R.M. Drake Jr, Analysis of heat and mass transfer, 1987.
[48] A.F. Mills, Basic heat and mass transfer, Prentice hall, 1999.
[49] G.F. Hewitt, G.L. Shires, T.R. Bott, Process heat transfer, vol. 113, CRC Press Boca Raton, FL, 1994.
[50] B. Sundén, Introduction to heat transfer, WIT Press, 2012.
[51] G. Hwang, C. Park, M. Kaviany, High-heat-flux distributed capillary artery evaporators, in: Handbook of Porous Media, CRC Press, 2015, pp. 615–648.
[52] K. Vafai, Handbook of porous media, Crc Press, 2015.
[53] I. Malavasi, B. Bourdon, P. Di Marco, J. De Coninck, M. Marengo, Appearance of a low superheat 'quasi-Leidenfrost' regime for boiling on superhydrophobic surfaces, Int. Commun. Heat Mass Transf. 63 (2015) 1–7.
[54] E. Teodori, T. Valente, I. Malavasi, A.S. Moita, M. Marengo, A.L.N. Moreira, Effect of extreme wetting scenarios on pool boiling conditions, Appl. Therm. Eng. 115 (2017) 1424–1437.
[55] B. Bourdon, P. Di Marco, R. Riobóo, M. Marengo, J. De Coninck, Enhancing the onset of pool boiling by wettability modification on nanometrically smooth surfaces, Int. Commun. Heat Mass Transf. 45 (2013) 11–15.
[56] B. Bourdon, E. Bertrand, P. Di Marco, M. Marengo, R. Rioboo, J. De Coninck, Wettability influence on the onset temperature of pool boiling: Experimental evidence onto ultra-smooth surfaces, Adv. Colloid Interface Sci. 221 (2015) 34–40.
[57] A.H. Howard, I. Mudawar, Orientation effects on pool boiling critical heat flux (CHF) and modeling of CHF for near-vertical surfaces, Int. J. Heat Mass Transf. 42 (9) (1999) 1665–1688.
[58] A. Faghri, Y. Zhang, Transport phenomena in multiphase systems, Elsevier, 2006.
[59] S. Mukherjee, I. Mudawar, Pumpless loop for narrow channel and micro-channel boiling, J. Electron. Packag. 125 (3) (2003) 431–441.
[60] S. Ishigai, K. Inoue, Z. Kiwaki, T. Inai, Boiling heat transfer from a flat surface facing downward, in: Proceedings of the International Heat Transfer Conference, 1961, pp. 224–229.
[61] Y. Katto, S. Yokoya, M. Yasunaka, Mechanism of boiling crisis and transition boiling in pool boiling, Int. Heat Transfer Conf. 4 (24) (1970).
[62] B.D. Marcus, D. Dropkin, The effect of surface configuration on nucleate boiling heat transfer, Int. J. Heat Mass Transf. 6 (9) (1963) 863–866.
[63] N. Kaneyasu, F. Yasunobu, U. Satoru, O. Haruhiko, Effect of surface configuration on nucleate boiling heat transfer, Int. J. Heat Mass Transf. 27 (9) (1984) 1559–1571.
[64] Z. Guo, M.S. El-Genk, An experimental study of saturated pool boiling from downward facing and inclined surfaces, Int. J. Heat Mass Transf. 35 (9) (1992) 2109–2117.
[65] A.A. Gribov, G.S. Taranov, N.M. Turchin, A.A. Tsyganok, Heat transfer and limiting heat loads in water boiling on downward-facing plane and spherical surfaces, Heat Transf. Res. 25 (6) (1993) 754–759.
[66] V.S. Granovskii, A.A. Sulatskiy, S.M. Shmelev, The crisis of nucleate boiling on a horizontal surface facing downward, Teplofiz. Vysok. Temp. 32 (1) (1994) 79–82.
[67] T.Y. Chu, B.L. Bainbridge, R.B. Simpson, J.H. Bentz, Ex-vessel boiling experiments: laboratory-and reactor-scale testing of the flooded cavity concept for in-vessel core retention Part I: Observation of quenching of downward-facing surfaces, Nucl. Eng. Des. 169 (1–3) (1997) 77–88.
[68] S.H. Yang, W.-P. Baek, S.H. Chang, Pool-boiling critical heat flux of water on small plates: effects of surface orientation and size, Int. Commun. Heat Mass Transf. 24 (8) (1997) 1093–1102.
[69] M.-G. Kang, Effects of tube inclination on pool boiling heat transfer, Nucl. Eng. Des. 220 (1) (2003) 67–81.
[70] M.-G. Kang, Effect of tube inclination on pool boiling heat transfer, J Heat Transf. 122 (1) (1999) 188–192.
[71] S. Jung, H. Kim, Effects of surface orientation on nucleate boiling heat transfer in a pool of water under atmospheric pressure, Nucl. Eng. Des. 305 (2016) 347–358.
[72] J.Y. Chang, S.M. You, Heater orientation effects on pool boiling of micro-porous-enhanced surfaces in saturated FC-72, J. Heat Transf. 118 (4) (1996) 937–943.
[73] F. Demiray, J. Kim, Microscale heat transfer measurements during pool boiling of FC-72: effect of subcooling, Int. J. Heat Mass Transf. 47 (14–16) (2004) 3257–3268.
[74] A. Faghri, Heat pipe science and technology, Global Digital Press (1995).
[75] M.J. Rightley, C.P. Tigges, R.C. Givler, C.V. Robino, J.J. Mulhall, P.M. Smith, Innovative wick design for multi-source, flat plate heat pipes, Microelectron. J. 34 (3) (2003) 187–194.
[76] L.-H. Chien, C.-C. Chang, Experimental study of evaporation resistance on porous surfaces in flat heat pipes, in: ITherm 2002. Eighth Intersociety Conference on Thermal and Thermomechanical Phenomena in Electronic Systems (Cat. No. 02CH37258), 2002, pp. 236–242.
[77] Y. Nam, S. Sharratt, G. Cha, Y.S. Ju, Characterization and modeling of the heat transfer performance of nanostructured Cu micropost wicks, J. Heat Transf. 133 (10) (2011), 101502.
[78] J.-H. Liou, C.-W. Chang, C. Chao, S.-C. Wong, Visualization and thermal resistance measurement for the sintered mesh-wick evaporator in operating flat-plate heat pipes, Int. J. Heat Mass Transf. 53 (7–8) (2010) 1498–1506.
[79] J.A. Weibel, S.V. Garimella, Visualization of vapor formation regimes during capillary-fed boiling in sintered-powder heat pipe wicks, Int. J. Heat Mass Transf. 55 (13–14) (2012) 3498–3510.
[80] G.S. Hwang, Y. Nam, E. Fleming, P. Dussinger, Y.S. Ju, M. Kaviany, Multi-artery heat pipe spreader: experiment, Int. J. Heat Mass Transf. 53 (13–14) (2010) 2662–2669.
[81] G.S. Hwang, et al., Multi-artery heat-pipe spreader: Lateral liquid supply, Int. J. Heat Mass Transf. 54 (11–12) (2011) 2334–2340.

[82] Y. Tang, D. Yuan, L. Lu, Z. Wang, A multi-artery vapor chamber and its performance, Appl. Therm. Eng. 60 (1–2) (2013) 15–23.
[83] C. Park, M. Crepinsek, Effect of operational conditions on cooling performance of pump-assisted and capillary-driven two-phase loop, J. Thermophys. Heat Transf. 25 (4) (2011) 572–580.
[84] M. Crepinsek, C. Park, Experimental analysis of pump-assisted and capillary-driven dual-evaporators two-phase cooling loop, Appl. Therm. Eng. 38 (2012) 133–142.
[85] T. Semenic, I. Catton, Experimental study of biporous wicks for high heat flux applications, Int. J. Heat Mass Transf. 52 (21–22) (2009) 5113–5121.
[86] J.A. Weibel, S.V. Garimella, M.T. North, Characterization of evaporation and boiling from sintered powder wicks fed by capillary action, Int. J. Heat Mass Transf. 53 (19–20) (2010) 4204–4215.
[87] S.M. You, Pool boiling heat transfer with highly wetting dielectric fluids, 1991.
[88] V.A. Grigoriev, V.V. Klimenko, Y.M. Pavlo, Y.V. Ametistov, A.V. Klimenko, Characteristic curve of helium pool boiling, Cryogenics 17 (3) (1977) 155–156.
[89] M.D. Reeber, Heat transfer to boiling helium, J. Appl. Phys. 34 (3) (1963) 481–483.
[90] G.R. Chandratilleke, S. Nishio, H. Ohkubo, Pool boiling heat transfer to saturated liquid helium from coated surface, Cryogenics 29 (6) (1989) 588–592.
[91] C. Schmidt, Review of steady state and transient heat transfer in pool boiling helium I, in: Stability of superconductors in helium I and helium II, 1981.
[92] P.J. Giarratano, N.V. Frederick, "Transient pool boiling of liquid helium using a temperature-controlled heater surface, Adv. Cryogenic Eng. Springer (1980) 455–466.
[93] D.N. Lyon, Boiling heat transfer and peak nucleate boiling fluxes in saturated liquidhelium between the ramda and critical temperatures, Adv. Cryog. Eng. 10 (1965) 371.
[94] L. Bewilogua, R. Knöner, H. Vinzelberg, Heat transfer in cryogenic liquids under pressure, Cryogenics 15 (3) (1975) 121–125.
[95] S.S. Kutateladze, Teploperedacha pri kondensatsii i kipenii [Heat transfer in Condensation and Boiling Conditions], Mosc. Gos. Nauchno-Tekhnicheskoe Izd. Mashinostroitelnoy Lit. (1952).
[96] I.P. Vishnev, M.E. Lebedev, A.I. Moroz, Terminology in cryogenics technology, Khim Neft Mashinostr no. 6 (1972) 38.
[97] M. Jergel, R. Stevenson, Heat transfer to boiling helium from aluminium surfaces, Electrotechnical Inst Bratislava (1972).
[98] M. Jergel, R. Stevenson, Static heat transfer to liquid helium in open pools and narrow channels, Int. J. Heat Mass Transf. 14 (12) (1971) 2099–2107.
[99] P.M. Githinji, R.H. Sabersky, Some effects of the orientation of the heating surface in nucleate boiling, J. Heat Transf. US 85 (1963).
[100] M. Misale, G. Guglielmini, A. Priarone, HFE-7100 pool boiling heat transfer and critical heat flux in inclined narrow spaces, Int. J. Refrig. 32 (2) (2009) 235–245.
[101] I.I. Gogonin, S.S. Kutateladze, Critical heat flux as a function of heater size for a liquid boiling in a large enclosure, J. Eng. Phys. Thermophys. 33 (5) (1977) 1286–1289.
[102] M.S. El-Genk, H. Bostanci, Saturation boiling of HFE-7100 from a copper surface, simulating a microelectronic chip, Int. J. Heat Mass Transf. 46 (10) (2003) 1841–1854.
[103] S. Jun, J. Kim, S.M. You, H.Y. Kim, Effect of heater orientation on pool boiling heat transfer from sintered copper microporous coating in saturated water, Int. J. Heat Mass Transf. 103 (2016) 277–284.
[104] W.M. Rohsenow, A method of correlating heat transfer data for surface boiling of liquids, MIT Division of Industrial Cooporation, Cambridge, Mass, 1951.
[105] N. Kurul and M. Z. Podowski, "Multidimensional effects in forced convection subcooled boiling," 1990.
[106] M. Lemmert, Influence of Flow Velocity on Surface Boiling Heat Transfert Coefficient, 1972.
[107] R. Cole, A photographic study of pool boiling in the region of the critical heat flux, AIChE J. 6 (4) (1960) 533–538.
[108] V.I. Tolubinsky, D.M. Kostanchuk, Vapour bubbles growth rate and heat transfer intensity at subcooled water boiling, Int. Heat Transfer Conf. 23 (4) (1970).
[109] S.S. Kutateladze, On the transition to film boiling under natural convection, Kotloturbostroenie 3 (1948) 10–12.
[110] N. Zuber, The hydrodynamic crisis in pool boiling of saturated and subcooled liquids, Int. Dev. Heat Transf. ASME 27 (1961) 230–236.
[111] I. Mudawar, A.H. Howard, C.O. Gersey, An analytical model for near-saturated pool boiling critical heat flux on vertical surfaces, Int. J. Heat Mass Transf. 40 (10) (1997) 2327–2339.
[112] S.J. Reed, I. Mudawar, Enhancement of boiling heat transfer using highly wetting liquids with pressed-on fins at low contact forces, Int. J. Heat Mass Transf. 40 (10) (1997) 2379–2392.
[113] I.P. Vishnev, Effect of orienting the hot surface with respect to the gravitational field on the critical nucleate boiling of a liquid, J. Eng. Phys. 24 (1) (1973) 43–48.
[114] M.S. El-Genk, Z. Guo, Transient boiling from inclined and downward-facing surfaces in a saturated pool, Int. J. Refrig. 16 (6) (1993) 414–422.
[115] M.J. Brusstar, H. Merte Jr, Effects of heater surface orientation on the critical heat flux—II. A model for pool and forced convection subcooled boiling, Int. J. Heat Mass Transf. 40 (17) (1997) 4021–4030.
[116] M. Arik, A. Bar-Cohen, Ebullient cooling of integrated circuits by Novec fluids, in: Proc. Pacific Rim Intersociety, Electronics Packaging Conference, 2001, pp. 18–23.
[117] L. Liao, R. Bao, Z. Liu, Compositive effects of orientation and contact angle on critical heat flux in pool boiling of water, Heat Mass Transf. 44 (12) (2008) 1447–1453.
[118] H. Hu, J.A. Weibel, S.V. Garimella, A coupled wicking and evaporation model for prediction of pool boiling critical heat flux on structured surfaces, Int. J. Heat Mass Transf. 136 (2019) 373–382.
[119] D.E. Kim, D.I. Yu, S.C. Park, H.J. Kwak, H.S. Ahn, Critical heat flux triggering mechanism on micro-structured surfaces: Coalesced bubble departure frequency and liquid furnishing capability, Int. J. Heat Mass Transf. 91 (2015) 1237–1247.
[120] K.-H. Chu, Y. Soo Joung, R. Enright, C.R. Buie, E.N. Wang, Hierarchically structured surfaces for boiling critical heat flux enhancement, Appl. Phys. Lett. 102 (15) (2013), 151602.
[121] K.-H. Chu, R. Enright, E.N. Wang, Structured surfaces for enhanced pool boiling heat transfer, Appl. Phys. Lett. 100 (24) (2012), 241603.
[122] S.G. Kandlikar, Controlling bubble motion over heated surface through evaporation momentum force to enhance pool boiling heat transfer, Appl. Phys. Lett. 102 (5) (2013), 051611.
[123] M.M. Rahman, E. Olceroglu, M. McCarthy, Role of wickability on the critical heat flux of structured superhydrophilic surfaces, Langmuir 30 (37) (2014) 11225–11234.
[124] S.H. Kim, G.C. Lee, J.Y. Kang, K. Moriyama, M.H. Kim, H.S. Park, Boiling heat transfer and critical heat flux evaluation of the pool boiling on micro structured surface, Int. J. Heat Mass Transf. 91 (2015) 1140–1147.
[125] H.J. Kwak, J.H. Kim, B.-S. Myung, M.H. Kim, D.E. Kim, Behavior of pool boiling heat transfer and critical heat flux on high aspect-ratio microchannels, Int. J. Therm. Sci. 125 (2018) 111–120.
[126] S. Sarangi, J.A. Weibel, S.V. Garimella, Quantitative evaluation of the dependence of pool boiling heat transfer enhancement on sintered particle coating characteristics, J. Heat Transf. 139 (2) (2017).
[127] A. Mehralizadeh, S.R. Shabanian, G. Bakeri, Effect of modified surfaces on bubble dynamics and pool boiling heat transfer enhancement: A review, Therm. Sci. Eng. Prog. 15 (2020), 100451.
[128] S. Swain, A. Swain, S.P. Kar, Influence of different surface coatings on pool boiling heat transfer enhancement: A brief review, Mater. Today Proc. 26 (2020) 1903–1907.
[129] Y.-W. Lu, S.G. Kandlikar, Nanoscale surface modification techniques for pool boiling enhancement—a critical review and future directions, Heat Transf. Eng. 32 (10) (2011) 827–842.
[130] C.M. Patil, S.G. Kandlikar, Review of the manufacturing techniques for porous surfaces used in enhanced pool boiling, Heat Transf. Eng. 35 (10) (2014) 887–902.
[131] W. Li, R. Dai, M. Zeng, Q. Wang, Review of two types of surface modification on pool boiling enhancement: Passive and active, Renew. Sustain. Energy Rev. 130 (2020), 109926.
[132] V.I. Deev, V.E. Keilin, I.A. Kovalev, A.K. Kondratenko, V.I. Petrovichev, Nucleate and film pool boiling heat transfer to saturated liquid helium, Cryogenics 17 (10) (1977) 557–562.
[133] S. Nishio, G.R. Chandratilleke, Steady-state pool boiling heat transfer to saturated liquid helium at atmospheric pressure, JSME Int. J. Ser 2 Fluids Eng. Heat Transf. Power Combust. Thermophys. Prop. 32 (4) (1989) 639–645.
[134] S.M. Kwark, M. Amaya, R. Kumar, G. Moreno, S.M. You, Effects of pressure, orientation, and heater size on pool boiling of water with nanocoated heaters, Int. J. Heat Mass Transf. 53 (23–24) (2010) 5199–5208.
[135] M. Borumand, G. Hwang, Enhanced pool boiling critical heat flux on tilted heating surfaces using columnar-post wick, in: ASME 2021 Int. Mech. Eng. Congr. Expo. IMECE, no. IMECE-2021-70054.
[136] D.S. Jung, J.E.S. Venart, A.C.M. Sousa, Effects of enhanced surfaces and surface orientation on nucleate and film boiling heat transfer in R-11, Int. J. Heat Mass Transf. 30 (12) (1987) 2627–2639.
[137] Y.H. Kim, K.Y. Suh, One-dimensional critical heat flux concerning surface orientation and gap size effects, Nucl. Eng. Des. 226 (3) (2003) 277–292.
[138] M. Monde, H. Kusuda, H. Uehara, Critical heat flux during natural convective boiling in vertical rectangular channels submerged in saturated liquid, 1982.
[139] G.P. Narayan, K.B. Anoop, G. Sateesh, S.K. Das, Effect of surface orientation on pool boiling heat transfer of nanoparticle suspensions, Int. J. Multiph. Flow 34 (2) (2008) 145–160.
[140] D. Wen, Y. Ding, Experimental investigation into the pool boiling heat transfer of aqueous based γ-alumina nanofluids, J. Nanoparticle Res. 7 (2–3) (2005) 265–274.
[141] H. Kim, M. Kim, Experimental study of the characteristics and mechanism of pool boiling CHF enhancement using nanofluids, Heat Mass Transf. 45 (7) (2009) 991–998.
[142] V. Trisaksri, S. Wongwises, Nucleate pool boiling heat transfer of TiO2–R141b nanofluids, Int. J. Heat Mass Transf. 52 (5–6) (2009) 1582–1588.
[143] R. Kamatchi, S. Venkatachalapathy, Parametric study of pool boiling heat transfer with nanofluids for the enhancement of critical heat flux: a review, Int. J. Therm. Sci. 87 (2015) 228–240.
[144] S.M. Kwark, R. Kumar, G. Moreno, J. Yoo, S.M. You, Pool boiling characteristics of low concentration nanofluids, Int. J. Heat Mass Transf. 53 (5–6) (2010) 972–981.
[145] D. Milanova, R. Kumar, Role of ions in pool boiling heat transfer of pure and silica nanofluids, Appl. Phys. Lett. 87 (23) (2005), 233107.
[146] S.J. Kim, I.C. Bang, J. Buongiomo, L.W. Hu, Study of pool boiling and critical heat flux enhancement in nanofluids, 2007.
[147] S.J. Kim, I.C. Bang, J. Buongiorno, L.W. Hu, Surface wettability change during pool boiling of nanofluids and its effect on critical heat flux, Int. J. Heat Mass Transf. 50 (19–20) (2007) 4105–4116.

[148] R.A. Taylor, P.E. Phelan, Pool boiling of nanofluids: comprehensive review of existing data and limited new data, Int. J. Heat Mass Transf. 52 (23–24) (2009) 5339–5347.
[149] J.H. Lienhard, On the two regimes of nucleate boiling, J. Heat Transf. 107 (1) (1985) 262–264.
[150] P. Pontes, et al., Effect of pattern geometry on bubble dynamics and heat transfer on biphilic surfaces, Exp. Therm. Fluid Sci. 115 (2020), 110088.
[151] P. Pontes, R. Cautela, E. Teodori, A.S. Moita, A.L.N. Moreira, Experimental description of bubble dynamics and heat transfer processes occurring on the pool boiling of water on biphilic surfaces, Appl. Therm. Eng. 178 (2020), 115507.
[152] A.R. Motezakker, A.K. Sadaghiani, S. Celik, T. Larsen, L.G. Villanueva, A. Koşar, Optimum ratio of hydrophobic to hydrophilic areas of biphilic surfaces in thermal fluid systems involving boiling, Int. J. Heat Mass Transf. 135 (2019) 164–174.
[153] H. Jo, H.S. Park, M.H. Kim, Single bubble dynamics on hydrophobic–hydrophilic mixed surfaces, Int. J. Heat Mass Transf. 93 (2016) 554–565.